THEORETICAL INVESTIGATION OF BIOFILM DETACHMENT AND PROTECTION FROM KILLING USING A BACTERIUM LEVEL AUTOMATA MODEL

By

Stephen Michael Hunt

A dissertation submitted in partial fulfillment
of the requirements for the degree

of

Doctor of Philosophy

in

Engineering

MONTANA STATE UNIVERSITY
Bozeman, Montana

May 2004

APPROVAL

of a dissertation submitted by

Stephen Michael Hunt

This dissertation has been read by each member of the dissertation committee and has been found to be satisfactory regarding content, English usage, format, citations, bibliographic style, and consistency, and is ready for submission to the College of Graduate Studies.

Dr. Philip S. Stewart

Approved for the Department of Chemical Engineering

Dr. Ronald W. Larsen

Approved for the College of Graduate Studies

Dr. Bruce McLeod

STATEMENT OF PERMISSION TO USE

In presenting this thesis in partial fulfillment of the requirements for a doctoral degree at Montana State University, I agree that the library shall make it available to borrowers under the rules of the library. I further agree that copying of this dissertation is allowable only for scholarly purposes, consistent with "fair use" as prescribed in the U.S. Copyright Law. Requests for extensive copying or reproduction of the dissertation should be referred to Bell & Howell Information and Learning, 300 North Zeeb Road, Ann Arbor, Michigan 48106, to whom I have granted "the exclusive right to reproduce and distribute my dissertation in and from microform along with the non-exclusive right to reproduce and distribute me abstract in any format in whole or in part."

Stephen Michael Hunt

May 24, 2004

ACKNOWLEDGMENTS

I have been fortunate while at the Center for Biofilm Engineering to have been surrounded by a tremendous supporting cast of researchers. I would like to specifically thank my advisor Phil Stewart. His knowledge and insight provided the direction necessary to keep this project continually progressing. I would also like to thank Marty Hamilton whose sustained enthusiasm and interest in this project (albeit now as a curious observer) kept the modeling efforts at the Center for Biofilm Engineering alive long enough for this project to find me. Marty and Phil have been irreplaceable resources throughout the course of this work, and I am grateful for the contributions made by them to this project and my professional development. Their patience and support during the preparation of this dissertation is also greatly appreciated.

Ultimately crucial to the success of my graduate work was the unrelenting support of my family. My mother, whose sometimes foolish confidence in my ability to accomplish anything, provided the necessary motivation to push through difficult times. My daughter MacKenzie, whose tight grip on my heart has always kept life in its proper perspective. And my wife Dana, who has willingly come last, is once again first.

Support from the W. M. Keck Foundation, NIH award R01 GM67245-02 to PSS, and cooperative agreement EEC-8907039 between the National Science Foundation and Montana State University is also gratefully acknowledged.

TABLE OF CONTENTS

TABLE OF CONTENTS - CONTINUED

LIST OF TABLES

LIST OF FIGURES

LIST OF FIGURES - CONTINUED

ABSTRACT

This dissertation presents a three-dimensional dynamic, stochastic computer model of biofilm development, BacLAB, created to theoretically explore conjectures associated with biofilms. BacLAB simulates the life cycle of a biofilm by mimicking the physical and biological behavior of a system with a simple set of experimentally determined "rules" applied to the smallest possible biofilm unit (the cell). These rules, however, lead to patterns on a larger scale. Much as bacterial cells organize themselves in a biofilm as a response to individual spatial conditions, the resulting model structure is produced in a process of self-organization rather than by some predetermined plan for biofilm development.

Detachment of cells from a mature biofilm is an important process determining the accumulation of attached cells and allowing for dissemination of the organism. The mode by which cells detach is, therefore, a critical stage in the life cycle of biofilms. Initial simulation studies with BacLAB were used to investigate conjectures associated with detachment resulting from either the accumulation of a metabolic product or the depletion of a metabolic substrate. Results demonstrated that the typical simulated biofilm eventually attains a steady state where biofilm growth was counterbalanced by detachment with cell areal densities comparable to those in laboratory biofilms. Some of the phenomena predicted by BacLAB include sloughing, hollow cell clusters and gradients in solute concentration and growth rate.

BacLAB was also adapted to simulate the protection from killing by antimicrobial agents afforded to microorganisms in the biofilm state. It is believed that the reduced susceptibility of bacteria in biofilms is an important factor in the persistence of some chronic infections and the mechanisms of protection are only moderately understood. Because antimicrobials are thought be more effective in killing actively growing bacteria, the rate of killing was assumed to be proportional to the local concentration of the substrate. The results suggest that substrate limitation has the potential to contribute to the reduced antimicrobial susceptibility found in biofilms, but is not adequate by itself in explaining the log-term persistence of biofilm viability observed experimentally.

CHAPTER 1

INTRODUCTION

Bacteria represent the most successful form of life on the planet, in terms of total biomass and in terms of the variety and extent of habitats colonized (19). The theory that the predominant state of bacteria in the natural environment is that of multicellular biofilms on surfaces is gaining wide acceptance. However, biofilm research has always been a technologically-dependent endeavor: from Van Leewenhoek's discovery of bacteria (a dental biofilm) with a microscope of his own construction, to Jones et al. (37) examination of "slime layers" on trickling filters in a waste water treatment plant with scanning and transmission electron microscopy, to the very controlled investigations of today that manipulate the bacteria's genetic material and have the ability to look inside hydrated biofilms using confocal scanning laser microscopy. Advances in laboratory instrumentation and molecular biology have drastically changed our view of biofilms over the last three decades. No longer do we think of biofilms as a homogeneous community of sessile microbes. Rather, we now view biofilms as a heterogeneous community of microbes that have the ability to differentiate, communicate, cooperate, and deploy collective survival strategies similar to those of a multi-cellular organism.

Past and Present Biofilm Modeling

Due to the important role that biofilms play in many industrial processes, biofilm research has always had a strong engineering component. One such component has been

the use of mathematical models as a research tool. Models have been used in biofilm research since the early 1970's and the advances in biofilm modeling have paralleled both the progress in our understanding of biofilms and the computational tools used in developing the models.

Processes Incorporated in Biofilm Models

Given the enormous diversity of biofilms, it is convenient to think of a biofilm in terms of its fundamental processes. This is particularly true from a modeling standpoint. By identifying important biofilm processes that can be modeled and the relationships between the processes, a mechanistic model of a biofilm can be developed that assists us in our investigation of biofilms. The development of such a model is an iterative process. As our understanding of biofilms develops, so too does our understanding of what processes are relevant to the phenomena observed in biofilms.

Mechanistic model development of microbial biofilms was initiated by Atkinson and coworkers (5, 6), in response to a resurgence of interest in fixed film systems for wastewater treatment. The earliest model from this group focused on substrate utilization in trickling filters. The model assumed that the intrinsic reaction rate in the biofilm was first order (as a simplification to the Monod expression) and neglected internal mass transfer by assuming that the substrate fully penetrated the biofilm (i.e. substrate utilization was sufficiently slow in comparison to its diffusion into the biofilm) (5). Subsequent work by Atkinson and Davies (7) focused primarily on the effects of mass transfer within the biofilm and how to account for gradients in substrate concentration stemming from microbial growth that the classical Monod expression neglected. They

developed a pseudo-analytical solution for the reaction-diffusion problem within a biofilm for a single limiting substrate.

Williamson and McCarty (87) developed a similar model in which they conceptualized a biofilm attached to a flat plate with infinite length and width (Figure 1). This "model biofilm" could be defined by four elements: substratum, biofilm, boundary layer, bulk fluid. It was the first to account for the incomplete mixing in the liquid immediately adjacent to the biofilm by including calculations for external mass transfer resistance through a concentration boundary layer. An interesting feature to come out of this work was the idea of an active layer within the biofilm. It had been observed that the biofilm surface flux, J_0, did not increase with an increase in biofilm thickness beyond a certain critical depth. Once this critical depth had been reached the biofilm became diffusion limited. In their conceptual description of the biofilm (Figure 1-1), Williamson and McCarty identified two characteristic substrate profiles: metabolism limited and diffusion limited. It was for these two limiting cases that an analytical solution was developed.

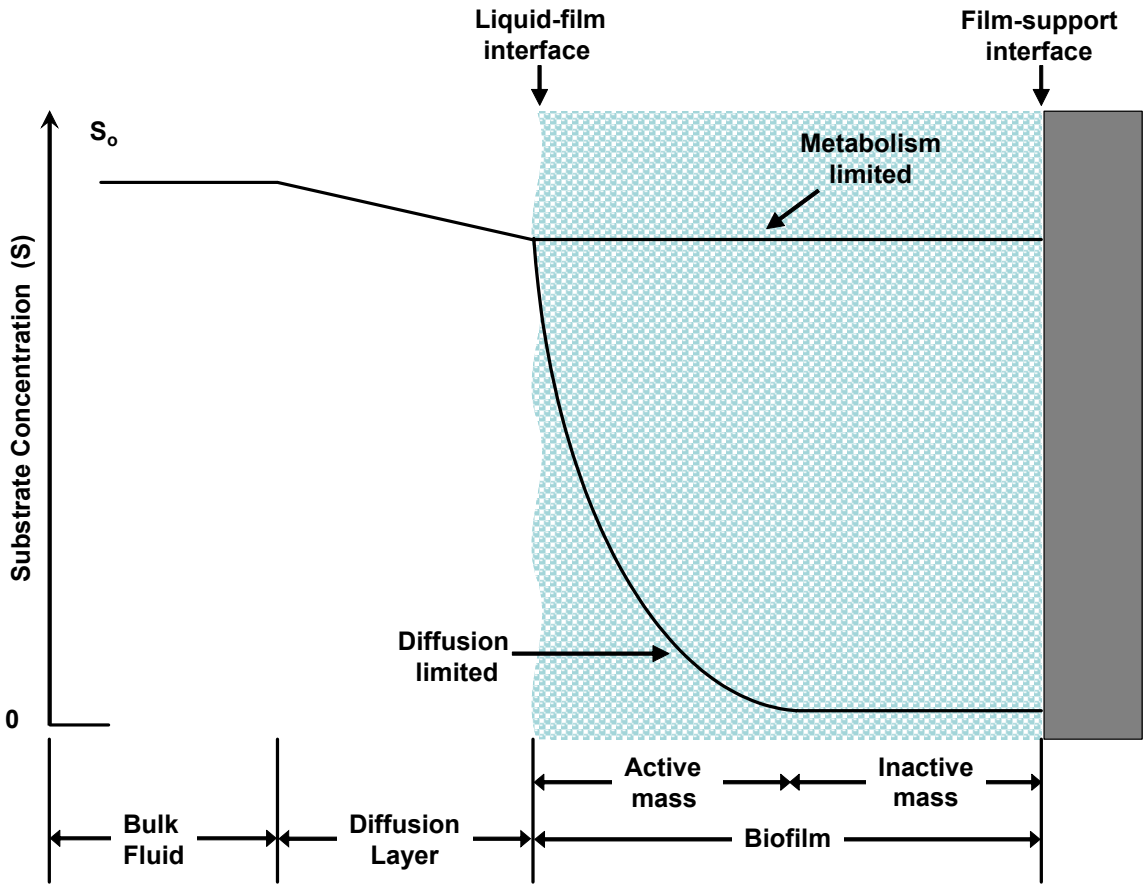

Figure 1-1. Conceptual basis for the biofilm model developed by Williamson and McCarty.

Despite the validity of these fundamental models, there was no expression for the interdependence between substrate utilization and biofilm mass. It is intuitive that high bulk substrate concentrations will produce thicker biofilms than those grown at low bulk substrate concentrations. The reasoning is that at high substrate concentrations the biofilm is better penetrated and the bacteria are able to capture chemical energy and convert it to biomass at a higher rate than if exposed to low substrate concentrations. Using this reasoning, Rittmann and McCarty (56, 57) incorporated expressions for bacterial growth and decay in a steady state biofilm by equating the expressions for these

two processes. The "steady state biofilm," as it was called, assumed the total amount of biofilm mass was just equal to that which could be supported by the substrate flux. This assumption allowed the thickness of a biofilm to be predicted from the bulk substrate concentration. It also predicted the minimum bulk substrate concentration needed to sustain a steady state biofilm, since the rate of energy capture would be less than the rate of energy expenditure needed to sustain the viability of the biofilm.

Biofilms are often not at steady state and grow or decay over time due to environmental fluctuations, making the ability to calculate the substrate flux into an unsteady state biofilm desirable. Building upon the previous work by Atkinson and Davies (7), Rittmann and McCarty (58) developed an unsteady state biofilm that explicitly included mass transport resistance. Thus, the substrate flux into the biofilm became a direct function of the bulk substrate concentration regardless of biofilm thickness. Unlike the steady state model, however, the unsteady state model requires that the biofilm thickness is known.

The ability to move away from limiting cases and pseudo-analytical solutions came with advances in computational resources and the idea of pseudo-steady state modeling. Pseudo-steady state modeling refers to the concept of separating fast processes from slow processes according to their characteristic time. Kissel et al. (38) identified that the processes of substrate uptake and diffusion within the biofilm are fast compared to microbial growth and decay, making it reasonable to model microbial growth and decay using steady state substrate concentration profiles. Updates to the concentration profiles are then calculated at regular intervals according to the

characteristic time used for microbial growth and decay. The pseudo-steady state approach optimizes the numerical solution of the model by allowing its characteristic time step to be that of microbial growth and decay. This optimization enabled biofilm models to evolve from describing a biofilm at a fixed moment in time to simulating the transient behavior of a biofilm.

The first models to use this approach were created independently by Kissel et al. (38) and Wanner and Gujer (83, 84). These models were developed to investigate species interaction in mixed culture biofilms. In addition to simulating a dynamic biofilm these models also included processes like detachment, attachment and the formation of inert biomass that could not be incorporated in the earlier static models. Furthermore the inclusion of multiple species within the biofilm also required the need to simulate biomass movement and the flux of multiple substrates through the biofilm.

Phenomena Simulated with Biofilm Models

The models developed by Kissel (38) et al. and Wanner and coworkers (84, 85) are somewhat of a turning point in the direction of biofilm modeling. Model development to this point was driven by the desire to more accurately predict phenomena of interest to industrial and wastewater systems (e.g., overall substrate utilization rate, biofilm thickness, minimum substrate concentration needed for biofilm growth, etc.). While these models are capable of accurately predicting these phenomena, they also provide insight into biofilm accumulation, species coexistence, species interactions and presence of niches within a biofilm. At this point, biofilm modeling had reached a level of maturity that enabled these models to be used as research tools to study different

phenomena observed in biofilms. Suddenly the objective in biofilm modeling was describing and predicting the phenomena observed experimentally.

Using a model based on the conceptual and mathematical formulation described by Wanner and Gujer (84), Stewart and coworkers (60, 70, 75) investigated processes like poor penetration of an antibiotic, physiological resistance to an antibiotic due to reduced bacterial growth rate, and the existence of a damaged cell state to explain the phenomena of a biofilm's reduced susceptibility to antibiotics. Other models have been used to investigated such things as pH effects within biofilms (22, 27), biofilm formation (36), and quorum sensing (23, 34, 47).

During the 1990's the general view on biofilm structure changed dramatically. The use of modern microscopes and computerized image analysis tools uncovered a much more complex biofilm morphology than could be captured with models developed to that time (15, 42). Thus to adequately capture this phenomena of structural heterogeneity, new modeling approaches needed to be developed in addition to the conventional continuum approaches used to this point.

Numerous groups were using discrete cellular automata methods to investigate the growth patterns of bacterial colonies with different random walk (9, 15, 42, 65, 66) and diffusion-limited aggregation models (28). Barker and Grimson (8) created a cellular automata model of microbial growth in which the diffusion and substrate utilization were represented by cellular automata algorithms. However, the first mentioned use of cellular automata in biofilm modeling was by Wimpenny and Colasanti (88) based on a previous work by Colasanti (18). Both this model and another developed independently by

Hermanowicz (33) used a simple cellular automata algorithm in two-dimensions that discretely represented biomass to capture the structural heterogeneity observed in real biofilms. Unlike previous models where the biofilm structure was used as input to the model, the structures obtained from these models was emergent from local interactions between the bacteria. The drawback in this approach was that results were not quantitative and could not be used to predict substrate fluxes and concentration gradients in the biofilm.

The idea of combining continuous and discrete models to simulate complex biological structures had been used previously to describe a variety of systems: activated sludge flocs (80), bacterial colonies on agar plates (9), filamentous fungi pellets (43), and slime mold crawling slugs (63). Picioreanu et al. (51, 53, 54) used this approach to create a two and three-dimensional model in which only the solid particle dynamics (i.e., bacteria, polymers, and support) were modeled discretely and the nutrient field solved using conventional differential equations. This type of discrete-differential modeling has all the capabilities of a conventional cellular automata model to describe the structural heterogeneity of a biofilm and can still predict substrate fluxes and concentration gradients from equations that contain well established microbial kinetics and mass transport terms. Later work from this group used the model to study the effect of convective transport on biofilm structure (52) and the role of internal stresses caused by fluid flow in causing detachment (55).

Kreft and coworkers (39-41) advanced the hybrid approach by adapting an individual-based simulator, Gecko (10, 67), for modeling ecosystem dynamics to the

study of microbial ecology. The Gecko framework models the individual agents, the bacteria, as free moving spheres not restricted to the computational lattice used in conventional cellular automata. The agents shove each other to simulate the pressure generated by a growing biofilm to avoid the overlap of cells. This approach makes it unnecessary to assume a biomass density or maximum biomass density *a priori.* Furthermore, the absence of any fixed lattice for the agents and the shoving algorithm used to simulate biofilm growth allow the production of EPS to be simulated by specifying how close individual bacteria can be to one another. Results have demonstrated that individual based modeling is very well suited to describing multi-species, multi-substrate biofilms that have complex structure.

Model Complexity

A biofilm model is simply a mathematical abstraction of a biofilm system. It provides a systematic mechanism by which a biofilm can be "reverse engineered" or recreated based on our current understanding of biofilms. Depending on the model's purpose, abstraction also allows for simplification of the system because often it is not necessary or even desired to have the model be exact or replicate all mechanisms exactly. For these reasons, models of varying degrees of complexity are constructed to study the complex interactions involving a variety of biofilm processes.

Early biofilm models averaged out the spatial heterogeneity by treating the biofilm as homogeneous flat slabs and focused on predicting the rate of substrate utilization. From a practical standpoint, there is no need to raise the level of complexity of the models used in most engineering applications. These seemingly simple models are

still appropriate to a variety of industrial and wastewater systems where meso-scale (i.e., on the order of millimeters) behavior of a biofilm is of interest and these models are still being developed today albeit at a much slower rate (59, 61, 62).

The evolution of biofilm models from one dimension to two and three dimensions has reduced the scale to which these models are applicable due to increased computational requirements. These models are more suited to biofilm research than industrial application as they simulate the micro-scale (i.e., on the order of micrometers) behavior of a biofilm. One advantage to these models is the ability to include conjectured processes into a model to provide insight as to what phenomena could be attributed to them.

When constructing a model, it is important to identify how the model will be used and what insight is to be gained from it. In doing so, a model containing all relevant processes and the appropriate level of complexity can be formulated.

Biofilm Processes and Phenomena of Interest

Detachment

Biofilm detachment refers to the inter-phase transport of biomass particles from the biofilm into the fluid wetting the film (73). Detachment is the major microbial process offsetting biofilm growth and, thus, regulates the steady state accumulation of the biofilm. However, detachment is the least studied biofilm process and very little is known about it. This can be attributed to the fact that although detachment is a temporally continuous process, it is spatially discrete and often difficult to observe. The

natural detachment of cells from biofilms has been divided into two broad categories: erosion and sloughing (13, 17). Erosion is the continuous departure of individual cells or small clusters of cells from the biofilm surface. Sloughing is a more discrete process where relatively large particles consisting of microbes held together by EPS detach. The distinction between erosion and sloughing is somewhat arbitrary because the distribution of particles departing the biofilm spans a continuum of sizes. It is generally accepted that erosion and sloughing result from a combination of biofilm process and shear and normal forces exerted by the moving fluid in contact with the biofilm surface.

Detachment plays a major role in the ecology of a biofilm. When organisms detach, either as individual particles or part of a clump, they have the potential to inoculate a suspended cell population or reattach downstream colonizing a previously unoccupied surface. The ability of cells to detach and become re-entrained within a biofilm provides a means for interaction between suspended cells and cells within the biofilm. The process of detachment coupled with reduced susceptibility to antimicrobials is a plausible strategy for the long term survival of bacteria. Furthermore, this process may by a key mechanism in recurrent medical infections and biofouling in drinking water distribution systems.

A variety of factors have been suggested to be important in biofilm detachment: shear and normal forces exerted by the fluid (49, 55, 78), matrix degrading enzymes (2, 11, 82), microbial generated gas bubbles (48), nutrient starvation and microbial growth status (4, 35, 50, 64, 68, 73), availability of multivalent cross-linking cations (4, 14, 81), contact attrition (16), and quorum sensing (1, 2, 32, 34), and the activation of a lytic

bacteriophage (86). New methods need to be developed to identify the primary factors involved in biofilm detachment and the specific processes(s) associated with these factors.

Reduced Susceptibility to Antimicrobials

Increased antimicrobial resistance is a phenomena commonly observed in microbial biofilms (20, 44, 46, 74). The reasons for the increased resistance are still mostly unknown. However, several mechanisms have been suggested to account for the recalcitrant nature of a biofilm when challenged with an antimicrobial agent: failure of the agent to penetrate the full depth of the biofilm, nutrient limitation and slow growth, and the existence of a protected phenotype within the biofilm (12, 24, 29, 31, 72).

Many antimicrobial agents that do not experience a reaction within the biofilm have been shown to adequately penetrate biofilms (3, 26, 76, 79, 89). However, if the antimicrobial agent is neutralized by a reaction or binds to the EPS matrix as it diffuses, concentration gradients of the antimicrobial agent would form in the biofilm. Antimicrobial agents like chlorine, hydrogen peroxide, and β-lactam antibiotics have been shown to have penetration reduced as a result of reaction within the biofilm (3, 21, 45, 74, 77).

Nutrient limitation and variations in growth rate within biofilms have been well documented. This combined with the fact that slow-growing and non-growing bacteria have been shown to be less susceptible to many antimicrobial agents provides a compelling mechanism for biofilm resistance (30). Experimental tests are consistent with

the idea of resistance due to slow growth and suggest that such a mechanism could partially account for an increased resistance to antimicrobial agents.

The idea of a protected phenotype or "persister cell" consists of a hypothetical cell state in which microorganisms are protected from antimicrobial challenges (25, 69, 71). The idea is that a small percentage of bacteria within a biofilm (< 1%) exist in this protected state but this protected subpopulation is capable of recultivating the biofilm in the event of a chemical or physical challenge that would otherwise eradicate the biofilm. Kill-versus-time curves typically exhibit tailing after prolonged exposure to an antimicrobial which is consistent with the theory of a protected phenotype.

Alone or together these and other proposed mechanisms are thought to contribute to reduced susceptibility of biofilm bacteria to antimicrobial agents. Computer models have been used to study different mechanisms of resistance with good success and the use of new models could continue to provide new insight into the mechanisms of protection in biofilms.

Scope of this Thesis

The scope of this thesis it to develop a three-dimensional biofilm model that is well adapted for investigating conjectures about biological mechanisms. This type of model must control the biofilm at its fundamental unit, the cell, and include all fundamental biofilm processes like diffusional transport of solutes, substrate consumption, microbial growth, microbial movement and detachment. Furthermore, the model should allow the aggregate behavior of the biofilm to be emergent from local

interactions among the bacteria making up the biofilm. The goal of this modeling work is to develop a biofilm model that facilitates communication across discipline boundaries through the use of cellular automata biofilm model.

In this thesis, the model will be used to test and evaluate the conjectures of a chemically mediated detachment mechanism (quorum sensing), detachment due to nutrient starvation, and antimicrobial resistance due to nutrient limitation and slow growth.

Modeling Approach

The conventional "bottom up" approach to modeling, based on physical laws, is well established and has the advantage of being able to quantitatively reproduce results. These advantages, however, do come at a cost. It is often computationally expensive to solve these models that typically are large systems of nonlinear partial differential equations. Furthermore, it is difficult to adapt these models to different experimental conditions making them impractical to use as a research tool. These often obstinate systems can, however, be made tractable by employing a modeling approach known as cellular automata.

A cellular automaton consists of a large assemblage of mutually and typically nonlinearly interacting identical parts that are discrete in time, space and state. Biological systems (and more specifically biofilms) are favorable for such a modeling approach because the aggregate behavior of a cellular automaton is in fact emergent, much like that of a biofilm. That is, the properties of the whole are not held by, nor can they be acquired

from, any of the constituent parts much like a single bacterial cell does not exhibit the properties of a biofilm.

Detailed knowledge of a number of mechanisms related to biofilm development is currently not complete and in many instances cannot be precisely quantified, making the "bottom up" approach a bit premature at the bacterial level. In contrast, a cellular automaton mimics the behavior at the cellular level by a simple set of easy to compute "rules" derived experimentally. These rules are commonly in the form of a look-up table relating the future state of a discrete segment of the model space (length, area, or volume depending on the model's dimension) to its current state and the state of any neighboring segments. Rules based upon experimentation have the added benefit of bridging the gap between the laboratory and the model. By driving model development through experimental data and observations, the model is flexible for testing conjectures stemming from laboratory research. In the final analysis, a model is judged by a single, quite pragmatic, factor: the model's usefulness.

The model developed in this work, BacLAB, describes the dynamic, stochastic behavior of a bacterial biofilm on a surface in an aqueous environment. BacLAB blends a conventional deterministic differential equations model for chemical reaction and diffusion with a stochastic cellular automata model for bacterial cell division, detachment and movement. The scale of the modeling domain is held such that it is suitable for describing the local environment of an individual bacterium in a biofilm colony. The unique feature of BacLAB is the ability to include a variety of hypothetical mechanisms making it suitable for use as a research tool.

Research Objectives

- Develop a three-dimensional, dynamic, stochastic computer model that is well suited to investigate a variety of conjectures about how specific processes at the biological level affect biofilm structure and/or function.
- Theoretically investigate the implications of detachment resulting from the accumulation of a bacterially derived detachment factor that initiates biofilm detachment.
- Theoretically investigate the implications of detachment resulting from the depletion of a metabolic substrate.
- Theoretically investigate the level of protection that could be explained by substrate limitation when a biofilm is exposed to a substrate-dependent antimicrobial agent.

References

1. **Allison, D. G., H. S. J. D., W. L., H. J., and G. P.** 1999. Cellular detachment and dispersal from bacterial biofilms: A role for quorum sensing?, p. 279-286. *In* P. G. J. Wimpenny, J. Walker, M. Brading, and R. Bayston (ed.), Biofilms: The Good, The Bad and The Ugly. Bioline, Cardiff, UK.

2. **Allison, D. G., B. Ruiz, C. SanJose, A. Jaspe, and P. Gilbert.** 1998. Extracellular products as mediators of the formation and detachment of Pseudomonas fluorescens biofilms. FEMS Microbiol. Lett. **167:**179-184.

3. **Anderl, J. N., M. J. Franklin, and P. S. Stewart.** 2000. Role of antibiotic penetration limitation in *Klebsiella pneumoniae* biofilm resistance to ampicillin and ciprofloxacin. Antimicrob. Agents Chemother. **44:**1818-1824.

4. **Applegate, D. H., and J. D. Bryers.** 1991. Effects of carbon and oxygen limitations and calcium concentrations on biofilm removal processes. Biotechnol. Bioeng. **37:**17-25.

5. **Atkinson, B., A. W. Busch, and G. S. Dawkins.** 1963. Recirculation, reaction kinetics, and effluent quality in a trickling filter flow model. Trans. Inst. Chem. Engrs. **35:**1307-1317.

6. **Atkinson, B., and I. S. Daoud.** 1970. Diffusion Effects within Microbial Films. Trans Inst Chem Eng **48:**T245-&.

7. **Atkinson, B., and I. J. Davies.** 1974. The overall rate of substrate uptake (reaction) by microbial films. Part I - A biological rate equation. Trans. Inst. Chem. Engrs. **52:**248-259.

8. **Barker, G. C., and M. J. Grimson.** 1993. A cellular automaton model of microbial growth. Binary **5:**132-137.

9. **Ben-Jacob, E., O. Schochet, A. Tenenbaum, I. Cohen, A. Czirók, and T. Vicsek.** 1994. Generic modelling of cooperative growth patterns in bacterial colonies. Nature **368:**46-49.

10. **Booth, G.** 1997. Gecko: a continuous 2D world for ecological modeling. Artif. Life **3:**147-63.

11. **Boyd, A., and A. M. Chakrabarty.** 1994. Role of alginate lyase in cell detachment of *Pseudomonas aeruginosa*. Appl. Environ. Microbiol. **60:**2355-2359.

12. **Brown, M. R., D. G. Allison, and P. Gilbert.** 1988. Resistance of bacterial biofilms to antibiotics: a growth-rate related effect? J Antimicrob Chemother **22:**777-80.

13. **Bryers, J. D.** 1988. Modeling biofilm accumulation, p. 109-144. *In* M. I. Bazin and J. I. Prosser (ed.), Physiological models in microbiology, vol. 2. CRC, Boca Raton, FL.

14. **Caccavo, F., B. Frolund, F. V. Kloeke, and P. H. Nielsen.** 1996. Deflocculation of activated sludge by the dissimilatory Fe(III)-reducing bacterium Shewanella alga BrY. Appl. Environ. Microbiol. **62:**1487-1490.

15. **Caldwell, D. E., D. R. Korber, and J. R. Lawrence.** 1992. Confocal laser micrscopy and digital inage analysis in microbial ecology, p. 1-67. *In* K. C. Marshall (ed.), Microbial Ecology. Plenum Press, New York, N.Y.

16. **Chang, H. T., B. E. Rittmann, D. Amar, R. Heim, O. Ehlinger, and Y. Lesty.** 1991. Biofilm detachment mechanisms in a liquid-fluidized bed. Biotechnol. Bioeng. **38:**499-506.

17. **Characklis, W. G., and K. C. Marshall (ed.).** 1990. Biofilms. John Wiley & Sons, inc., New York.

18. **Colasanti, R. L.** 1992. Cellular automata models of microbial colonies. Binary **4:**191-193.

19. **Costerton, J. W., Z. Lewandowski, D. E. Caldwell, D. R. Korber, and H. M. Lappin-Scott.** 1995. Microbial biofilms. Annu. Rev. Microbiol. **49:**711-745.

20. **Davies, D.** 2003. Understanding biofilm resistance to antibacterial agents. Nature Reviews Drug Discovery **2:**114-122.

21. **de Beer, D., P. Stoodley, F. Roe, and Z. Lewandowski.** 1994. Effects of biofilm structures on oxygen distribution and mass-transport. Biotechnol. Bioeng. **43:**1131-1138.

22. **Dibdin, G. H.** 1992. A finite-difference computer-model of solute diffusion in bacterial films with simultaneous metabolism and chemical-reaction. Comput Appl Biosci **8:**489-500.

23. **Dockery, J. D., and J. P. Keener.** 2001. A mathematical model for quorum sensing in *Pseudomonas aeruginosa*. B. Math. Biol. **60:**95-116.

24. **Donlan, R. M., and J. W. Costerton.** 2002. Biofilms: survival mechanisms of clinically relevant microorganisms. Clin. Microbiol. Rev. **15:**167-93.

25. **Drenkard, E., and F. M. Ausubel.** 2002. Pseudomonas biofilm formation and antibiotic resistance are linked to phenotypic variation. Nature **416:**740-743.

26. **Dunne, W. M., E. O. Mason, and S. L. Kaplan.** 1993. Diffusion of rifampin and vancomycin through a *Staphylococcus-epidermidis* biofilm. Antimicrob. Agents Chemother. **37:**2522-2526.

27. **Flora, J. R. V., M. T. Suidan, P. Biswas, and G. D. Sayles.** 1993. Modeling Substrate Transport into Biofilms - Role of Multiple Ions and Ph Effects. J. Environ. Eng. ASCE **119:**908-930.

28. **Fujikawa, H.** 1994. Diversity of the growth patterns of *Bacillus subtilis* colonies on agar plates. FEMS Microbiol. Ecol. **13:**159-168.

29. **Gilbert, P., D. G. Allison, and A. J. McBain.** 2002. Biofilms in vitro and in vivo: do singular mechanisms imply cross-resistance? J. Appl. Microbiol. **92 Suppl:**98S-110S.

30. **Gilbert, P., and M. R. Brown.** 1995. Mechanisms of the protection of bacterial biofilms from antimicrobial agents, p. 118-130. *In* H. M. Lappin-Scott and J. W. Costerton (ed.), Microbial Biofilms. Cambridge University Press, Cambridge.

31. **Gilbert, P., T. Maira-Litran, A. J. McBain, A. H. Rickard, and F. W. Whyte.** 2002. The physiology and collective recalcitrance of microbial biofilm communities. Adv. Microb. Physiol. **46:**202-56.

32. **Hentzer, M., K. Riedel, T. B. Rasmussen, A. Heydorn, J. B. Andersen, M. R. Parsek, S. A. Rice, L. Eberl, S. Molin, N. Hoiby, S. Kjelleberg, and M. Givskov.** 2002. Inhibition of quorum sensing in *Pseudomonas aeruginosa* biofilm bacteria by a halogenated furanone compound. Microbiol. **148:**87-102.

33. **Hermanowicz, S. W.** 1998. A model of two-dimensional biofilm morphology. Wat. Sci. Tech. **37:**219-222.

34. **Hunt, S. M., M. A. Hamilton, J. T. Sears, G. Harkin, and J. Reno.** 2003. A computer investigation of chemically mediated detachment in bacterial biofilms. Microbiol. **149:**1155-63.

35. **Jackson, D. W., K. Suzuki, L. Oakford, J. W. Simecka, M. E. Hart, and T. Romeo.** 2002. Biofilm formation and dispersal under the influence of the global regulator CsrA of *Escherichia coli*. J. Bacteriol. **184:**290-301.

36. **Jones, D., H. V. Kojouharov, D. Le, and H. Smith.** 2003. The Freter model: A simple model of biofilm formation. J. Math. Biol. **47:**137-52.

37. **Jones, H. C., I. L. Roth, and W. M. Sanders III.** 1969. Electron microscopic study of a slime layer. J. Bacteriol. **99:**316–325.

38. **Kissel, J. C., P. L. McCarty, and R. L. Street.** 1984. Numerical simulation of mixed-culture biofilm. J. Environ. Eng. **110:**393-411.

39. **Kreft, J. U., G. Booth, and J. W. T. Wimpenny.** 1998. BacSim, a simulator for individual-based modelling of bacterial colony growth. Microbiol. **144:**3275-3287.

40. **Kreft, J. U., C. Picioreanu, J. W. Wimpenny, and M. C. van Loosdrecht.** 2001. Individual-based modelling of biofilms. Microbiol. **147:**2897-2912.

41. **Kreft, J. U., and J. W. Wimpenny.** 2001. Effect of EPS on biofilm structure and function as revealed by an individual-based model of biofilm growth. Wat. Sci. Tech. **43:**135-141.

42. **Lawrence, J. R., D. R. Korber, B. D. Hoyle, J. W. Costerton, and D. E. Caldwell.** 1991. Optical sectioning of microbial biofilms. J. Bacteriol. **173:**6558-67.

43. **Lejeune, R., and G. V. Baron.** 1997. Simulation of growth of a filamentous fungus in 3 dimensions. Biotechnol. Bioeng. **53:**139-150.

44. **Lewis, K.** 2001. Riddle of biofilm resistance. Antimicrob. Agents Chemother. **45:**999-1007.

45. **Lu, X., F. Roe, A. Jesaitis, Z. Lewandowski, and X. Liu.** 1998. Resistance of biofilms to the catalase inhibitor 3-amino-1,2, 4-triazole. Biotechnol. Bioeng. **59:**156-62.

46. **Mah, T. C., and G. A. O'Toole.** 2001. Mechanisms of biofilm resistance to antimicrobial agents. Trends Microbiol. **9:**34-39.

47. **Nilsson, P., A. Olofsson, M. Fagerlind, T. Fagerstrom, S. Rice, S. Kjelleberg, and P. Steinberg.** 2001. Kinetics of the AHL regulatory system in a model biofilm system: How many bacteria constitute a "quorum"? J. Mol. Biol. **309:**631-640.

48. **Ohashi, A., and H. Harada.** 1994. Characterization of detachment mode of biofilm developed in an attached-growth reactor. Wat. Sci. Tech. **30:**35-45.

49. **Peyton, B. M.** 1996. Effects of shear stress and substrate loading rate on *Pseudomonas aeruginosa* biofilm thickness and density. Wat. Res. **30:**29.

50. **Peyton, B. M., and W. G. Characklis.** 1993. Statistical analysis of the effect of substrate utilization and shear stress on the kinetics of biofilm detachment. Biotechnol. Bioeng. **41:**728-735.

51. **Picioreanu, C., M. C. M. van Loosdrecht, and J. J. Heijnen.** 1999. Discrete-differential modelling of biofilm structure. Wat. Sci. Tech. **39:**115-122.

52. **Picioreanu, C., M. C. M. van Loosdrecht, and J. J. Heijnen.** 2000. Effect of diffusive and convective substrate transport on biofilm structure formation: A two-dimensional modeling study. Biotechnol. Bioeng. **69:**504-515.

53. **Picioreanu, C., M. C. M. van Loosdrecht, and J. J. Heijnen.** 1998. Mathematical modeling of biofilm structure with a hybrid differential-discrete cellular automaton approach. Biotechnol. Bioeng. **58:**101-116.

54. **Picioreanu, C., M. C. M. van Loosdrecht, and J. J. Heijnen.** 1998. New combined differential-discrete cellular automaton approach for biofilm modeling: Application for growth in gel beads. Biotechnol. Bioeng. **57:**718-731.

55. **Picioreanu, C., M. C. M. van Loosdrecht, and J. J. Heijnen.** 2001. Two-dimensional model of biofilm detachment caused by internal stress from liquid flow. Biotechnol. Bioeng. **72:**205-218.

56. **Rittmann, B. E., and P. L. McCarty.** 1980. Evaluation of steady-state-biofilm kinetics. Biotechnol. Bioeng. **22**.

57. **Rittmann, B. E., and P. L. McCarty.** 1980. Model of steady-state-biofilm kinetics. Biotechnol. Bioeng. **22:**2343-2357.

58. **Rittmann, B. E., and P. L. McCarty.** 1981. Substrate flux into biofilms of any thickness. J. Environ. Eng. ASCE **107:**831-849.

59. **Rittmann, B. E., D. Stilwell, and A. Ohashi.** 2002. The transient-state, multiple-species biofilm model for biofiltration processes. Wat. Res. **36:**2342-2356.

60. **Roberts, M. E., and P. S. Stewart.** 2004. Modeling antibiotic tolerance in biofilms by accounting for nutrient limitation. Antimicrob. Agents Chemother. **48:**48-52.

61. **Saez, P. B., and B. E. Rittmann.** 1992. Accurate pseudoanalytical solution for steady-state biofilms. Biotechnol. Bioeng. **39:**790-793.

62. **Saez, P. B., and B. E. Rittmann.** 1992. Model-parameter estimation using least-squares. Wat. Res. **26:**789-796.

63. **Savill, N. J., and P. Hogeweg.** 1997. Modelling morphogenesis: From single cells to crawling slugs. J Theor Biol **184:**229-235.

64. **Sawyer, L. K., and S. W. Hermanowicz.** 1998. Detachment of biofilm bacteria due to variations in nutrient supply. Wat. Sci. Tech. **37:**211-214.

65. **Schindler, J., and T. Rataj.** 1992. Fractal geometry and growth models of *Bacillus* colony. Binary **4:**66-72.

66. **Schindler, J., and L. Rovensky.** 1994. A model of intrinsic growth of a *Bacillus* colony. Binary **6:**105-108.

67. **Schmitz, O. J., and G. Booth.** 1997. Modelling food web complexity: The consequences of individual-based, spatially explicit behavioural ecology on trophic interactions. Evol Ecol **11:**379-398.

68. **Speitel, G. E., and F. A. Digiano.** 1987. Biofilm shearing under dynamic conditions. J. Environ. Eng. ASCE **113:**464-475.

69. **Spoering, A. L., and K. Lewis.** 2001. Biofilms and planktonic cells of *Pseudomonas aeruginosa* have similar resistance to killing by antimicrobials. J. Bacteriol. **183:**6746-6751.

70. **Stewart, P. S.** 1994. Biofilm accumulation model that predicts antibiotic resistance of *Pseudomonas aeruginosa* biofilms. Antimicrob. Agents Chemother. **38:**1052-1058.

71. **Stewart, P. S.** 2004. Biofilm antimicrobial resistance. *In* G. Ghannoum and G. A. O'Toole (ed.), Microbial Biofilms. ASM Press, Washington, D.C.

72. **Stewart, P. S.** 2002. Mechanisms of antibiotic resistance in bacterial biofilms. Int. J. Med. Microbiol. **292:**107-113.

73. **Stewart, P. S.** 1993. Model of biofilm detachment. Biotechnol. Bioeng. **41:**111-117.

74. **Stewart, P. S., and J. W. Costerton.** 2001. Antibiotic resistance of bacteria in biofilms. Lancet **358:**135-138.

75. **Stewart, P. S., M. A. Hamilton, B. R. Goldstein, and B. T. Schneider.** 1996. Modeling biocide action against biofilms. Biotechnol. Bioeng. **49:**445-455.

76. **Stewart, P. S., J. Rayner, F. Roe, and W. M. Rees.** 2001. Biofilm penetration and disinfection efficacy of alkaline hypochlorite and chlorosulfamates. J. Appl. Microbiol. **91:**525-32.

77. **Stewart, P. S., F. Roe, J. Rayner, J. G. Elkins, Z. Lewandowski, U. A. Ochsner, and D. J. Hassett.** 2000. Effect of catalase on hydrogen peroxide penetration into *Pseudomonas aeruginosa* biofilms. Appl. Environ. Microbiol. **66:**836-8.

78. **Stoodley, P., S. Wilson, L. Hall-Stoodley, J. D. Boyle, H. M. Lappin-Scott, and J. W. Costerton.** 2001. Growth and detachment of cell clusters from mature mixed-species biofilms. Appl. Environ. Microbiol. **67:**5608-5613.

79. **Suci, P. A., M. W. Mittelman, F. P. Yu, and G. G. Geesey.** 1994. Investigation of ciprofloxacin penetration into *Pseudomonas-aeruginosa* biofilms. Antimicrob. Agents Chemother. **38:**2125-2133.

80. **Takacs, I., and E. Fleit.** 1995. Modeling of the Micromorphology of the Activated-Sludge Floc - Low Do, Low F/M Bulking. Wat. Sci. Tech. **31:**235-243.

81. **Turakhia, M. H., K. E. Cooksey, and W. G. Characklis.** 1983. Influence of a calcium-specific chelant on biofilm removal. Appl. Environ. Microbiol. **46:**1236-1238.

82. **Vats, N., and S. F. Lee.** 2000. Active detachment of *Streptococcus mutans* cells adhered to epon-hydroxylapatite surfaces coated with salivary proteins in vitro. Arch. Oral. Biol. **45:**305-314.

83. **Wanner, O., and W. Gujer.** 1985. Competition in Biofilms. Wat. Sci. Tech. **17:**27-44.

84. **Wanner, O., and W. Gujer.** 1986. Multispecies biofilm model. Biotechnol. Bioeng. **28:**314-328.

85. **Wanner, O., and P. Reichert.** 1996. Mathematical modeling of mixed-culture biofilms. Biotechnol. Bioeng. **49:**172-184.

86. **Webb, J. S., L. S. Thompson, S. James, T. Charlton, T. Tolker-Nielsen, B. Koch, M. Givskov, and S. Kjelleberg.** 2003. Cell death in *Pseudomonas aeruginosa* biofilm development. J. Bacteriol. **185:**4585-92.

87. **Williamson, K., and P. L. Mccarty.** 1976. Model of substrate utilization by bacterial films. J. Water Pollut. Con. F. **48:**9-24.

88. **Wimpenny, J. W. T., and R. Colasanti.** 1997. A unifying hypothesis for the structure of microbial biofilms based on cellular automaton models. FEMS Microbiol. Ecol. **22:**1-16.

89. **Zheng, Z. L., and P. S. Stewart.** 2002. Penetration of rifampin through *Staphylococcus epidermidis* biofilms. Antimicrob. Agents Chemother. **46:**900-903.

CHAPTER 2

A COMPUTER INVESTIGATION OF CHEMICALLY MEDIATED DETACHMENT IN BACTERIAL BIOFILMS

Reproduced with permission from **Hunt, S. M., M. A. Hamilton, J. T. Sears, G. Harkin, and J. Reno.** 2003. A computer investigation of chemically mediated detachment in bacterial biofilms. Microbiol. **149:**1155-63.

Summary

A three-dimensional computer model was used to evaluate the effect of chemically mediated detachment on biofilm development in a negligible-shear environment. Our model, BacLAB, combines conventional diffusion-reaction equations for chemicals with a cellular automata algorithm to simulate bacterial growth, movement and detachment. BacLAB simulates the life cycle of a bacterial biofilm from its initial colonization of a surface to the development of a mature biofilm with areal cell densities comparable to those in the laboratory. We have created a base model founded on well established transport equations that are easily adaptable to investigate conjectures at the biological level. In this paper we examined the conjecture of a detachment mechanism involving a bacterially produced chemical detachment factor in which high local concentrations of this detachment factor cause the bacteria to detach from the biofilm. The results show that the often observed mushroom-shaped structure can occur if detachment events create voids so that the remaining attached cells look like mushrooms.

Introduction

That multicellular biofilms on surfaces may be the predominant state of bacteria in the natural environment is gaining wide-spread acceptance. According to Watnick and Kolter (27), if taken to the extreme, we may view the planktonic, or free-swimming, phase primarily as a mechanism for translocating from one surface to another. For bacteria to avoid density-mediated starvation and to colonize new surfaces, cells must be able to leave the biofilm and disperse. This process of cell transfer from a mature biofilm to an unoccupied surface is a plausible strategy for the long-term survival of bacteria. The mode by which cells detach is, therefore, a critical stage in the life cycle of biofilms (22).

It is known that biofilms are heterogeneous structures from which both single cells and multicellular aggregates slough (23). Recently it has been suggested that freely diffusible chemical signals play an important role in biofilm development and maintenance (7, 13). Although the mechanisms have not been established, there is some experimental evidence that a subset of these chemical signals plays an active role in biofilm detachment (1, 3). Boyd & Chakrabarty (3) state that when expressed from a regulated promoter, alginate lyase can induce enhanced sloughing of cells due to degradation of the alginate.

Mathematical models have been used for the last three decades to synthesize and integrate our knowledge about the behavior of microbial biofilms. Early models represented biofilms as homogeneous steady-state films containing a single species (21).

They later evolved to dynamic multisubstrate-multispecies biofilm computer models (20, 25, 26). Although these models were advanced descriptions, they were governed exclusively by one-dimensional mass transport and biochemical interactions and the models could not account for the experimentally observed three-dimensional heterogeneity resulting from bacterial attachment, growth, and detachment. The morphology was essentially predetermined by the modeler. Detachment was represented by an arbitrary uniform removal rate or velocity. These models are generally suitable for representing aggregate biofilm activity on many square millimeters of surface area.

The subsequent generation of biofilm models focused on a smaller scale. Most utilized discrete methods, such as cellular automata, to simulate the rules that govern the lives of microbial cells. These models produced realistic, structurally heterogeneous biofilms (2, 6, 8, 9, 11, 14, 16, 18, 28). They allowed the artificial biofilm structure to evolve as a self-organization process, emulating how bacterial cells organize themselves into biofilms. Some models ignored detachment, while others viewed detachment as a process completely dependent on the shear stress induced by the flowing bulk liquid. No published models consider other potential detachment mechanisms.

The aim of this article is to evaluate the implications of a chemically mediated detachment mechanism through computer experimentation. We describe a three-dimensional biofilm model that combines conventional diffusion-reaction equations for chemicals to model solute transport and a cellular automata algorithm to simulate the bacterial growth, movement, and detachment. Three different plausible cellular automata detachment rules are examined by conducting 20 replicate simulations for each

detachment rule. Detachment via a hypothetical bacteria-produced chemical detachment factor produces structures compatible with the known morphology and dynamic behavior of biofilms. We conclude that the simulation results are both qualitatively and quantitatively similar to those for laboratory biofilms. The conjecture of a chemically mediated detachment mechanism is not invalidated.

Model Description

The present computer model, named BacLAB, describes the dynamic, stochastic behavior of a bacterial biofilm on a surface (substratum) in an aqueous environment. Although the bulk liquid is assumed to be well-mixed, it produces no shear-stress on the biofilm. BacLAB blends a conventional, deterministic differential equations model for chemical reaction and diffusion with a stochastic cellular automata model for bacterial cell division, detachment, and movement. The scale of the modeling domain, approximately 1 mm^2, is suitable for describing the local environment of an individual bacterium in a biofilm colony. The unique feature of BacLAB is its ability to include a chemical factor, produced by the bacteria, which leads to detachment when large local concentrations are achieved. The existence of such a detachment factor is an important conjecture (19), the implications of which are conveniently explored by computer experimentation with this model.

The Domain

The spatial domain, Γ, of the model consists of a box, typically 900 μm per side, containing two overlapping computational grids. The first grid is a fixed lattice used to

represent any soluble components (e.g. substrate, detachment factor) in the model. The second grid partitions the model space into many small cubes, each cube being a volume element large enough (here assumed 3 μm per side) to include a bacterial cell and its associated extracellular polymeric substance (EPS) (5). Coordinates of each cube and lattice point are then uniquely given by the set of vectors $\{(x,y,z)$ such that $x=0\ldots N_x-1$, $y=0\ldots N_y-1$, $z=0\ldots N_z-1\}$. There are $N_x \cdot N_y \cdot N_z$ total lattice points and cubes. In our simulations $N_x = N_y = N_z = 300$. Here $z=0$ indicates an element on the substratum, and $z=N_z-1$ indicates an element the furthest from the substratum. There is a one-to-one correspondence between lattice points and cubes.

The temporal domain is discrete with equally spaced time points, typically 1 h apart, chosen to be small with respect to biofilm development.

State Variables

At any time point three primary arrays are used to represent the state of the system: $S = \{ C_S(x,y,z) \}$, $F = \{ C_F(x,y,z) \}$, and $B = \{ B(x,y,z) \}$, where $C_S(x,y,z)$ denotes the concentration of the limiting substrate, $C_F(x,y,z)$ denotes the concentration of the detachment factor, and $B(x,y,z)$ denotes the occupation state at location (x,y,z).

Each element within the substrate and detachment arrays, $C_S(x,y,z)$ and $C_F(x,y,z)$, contains a positive real value corresponding to that solute's concentration at that node location. The occupation state of a cube, $B(x,y,z)$, is represented by an identity pointer to a vector, $I_{\text{bacterium}}$, containing all relevant information (e.g. bacterial species, kinetic parameters, etc.) about an individual bacterium. If the cube is unoccupied by a bacterium, it is represented by a null identity pointer. When computing the state of the

system at the next time point, S and F are updated using conventional differential equations, while B is updated using cellular automata rules.

Differential Equations for Solutes

In the aqueous environment being modeled, the bulk liquid is well-mixed, but imposes no shear-stress on the biofilm. The solutes are transported solely by diffusion in the biofilm. The concentrations $C_S(x,y,z)$ and $C_F(x,y,z)$ are a result of molecular diffusion and reaction (consumption or production) with the bacteria. The diffusional time constant is approximately 100 orders of magnitude smaller than that for bacterial cell division (17). Thus, molecular diffusion can be assumed to be at steady state with respect to the bacterial growth. Suppressing the location indices (x,y,z), let C_i denote the concentration of solute i, where i is either the limiting substrate, S, or chemical detachment factor, F. Let the parameter D_i denote the diffusivity coefficient of solute i. The diffusivity in the biofilm is calculated by multiplying the diffusivity of the solute in the aqueous or bulk phase, $D_{i,\mathrm{aq}}$ by the relative effective diffusivity, $D_{i,\mathrm{e}}/D_{i,\mathrm{aq}}$. The variable X denotes the biomass density (calculated as average cell mass per cube volume for occupied cubes and 0 otherwise), and $r_i(C_s,X)$ denotes the reaction term (to be defined below) corresponding to substrate i's consumption or production by the bacteria. A negative r_i indicates substrate conversion into biomass and a positive r_i indicates that the bacteria are producing the solute, as is the case for the chemical detachment factor. Equation (2-1) is the three-dimensional representation for diffusive transport and reaction.

$$0 = D_i\left(\frac{\partial^2 C_i}{\partial x^2} + \frac{\partial^2 C_i}{\partial y^2} + \frac{\partial^2 C_i}{\partial z^2}\right) + r_i(C_S, X) \tag{2-1}$$

Equation (2-2) is the classical Monod (15) equation for the substrate consumption by bacteria. Here $\mu_{\max}$ denotes the maximum specific growth rate, Y_{XS} denotes the yield coefficient, and K_S denotes the half saturation coefficient.

$$r_S(C_S, X) = \left(\frac{\mu_{\max} \cdot X}{Y_{XS}}\right)\left(\frac{C_S}{K_S + C_S}\right) \tag{2-2}$$

Using small time steps, Δt, relative to growth, we approximate the reaction term by calculating the reaction rate at the current time step, t. Using finite differences to approximate the derivative in Equation (2-1), the result is a three-dimensional block tridiagonal linear system. This system is then solved using a discrete fast Fourier transform for the concentration at $t+\Delta t$. The solver used was the pois3d subroutine from the FISHPAK library (available at http://www.netlib.org/fishpack/).

Let the parameter k denote the detachment factor production coefficient. Equation (2-3) is an assumed first order kinetic expression in C_S for the detachment factor production. This first order expression in C_S attempts to correlate the detachment factor production with cellular activity. It is therefore assumed that, when a cell is in a starved state, energy is conserved and extra cellular chemicals are not actively produced.

$$r_F(C_S, X) = \begin{cases} 0, & \text{if } B = \text{Null Identity Pointer} \\ k \cdot C_{S,} & \text{if } B \neq \text{Null Identity Pointer} \end{cases} \tag{2-3}$$

Equation (2-3), inserted into (2-1) for r_i, where C_i is the detachment factor concentration, C_F, again results in a three-dimensional block tridiagonal linear system and can be solved as indicated above.

The model's substrate uptake from the surrounding environment is dictated by the set of boundary conditions used in the simulation. The substratum is modeled as an impermeable surface by specifying a no flux boundary condition at z=0.

$$\left.\frac{dC_i}{dz}\right|_{z=o} = 0 \quad \text{for } i = S,\ F. \tag{2-4}$$

The substrate source is generated by maintaining a constant concentration of the substrate in the bulk fluid, $C_{S,\text{bulk}}$, at a fixed height above the top of the biofilm as a moving boundary. Conversely, a sink for the detachment factor is created by maintaining the concentration in the bulk fluid at zero, that is, $C_{F,\text{bulk}}$=0. This feature is reasonable if convective transport removes the detachment factor from locations in the bulk liquid above the top of the biofilm.

To eliminate edge effects, the model utilizes a periodic boundary in the x and y directions. For example, the periodic boundary condition implemented in the y direction means that the node (x,N_y-1,z) is a nearest neighbor to the node at $(x,0,z)$. Therefore, a particle going past the boundary on one side of the box results in the particle being wrapped back to the corresponding opposite side.

Cellular Automata Rules for Bacterial Behavior

Cellular automata rules are used to update the occupation array, B, at each time step. The rules are locally applied to each bacterium to determine its new state as a

function of local environment and the previous state of that bacterium. The rules specify whether each bacterium divides, moves, or detaches.

Let the parameter m_{avg} denote the average mass of an individual bacterium. For a bacterium to divide it must consume enough substrate to create a new daughter cell ($\approx [(m_{avg})/(Y_{XS})]$). Therefore, each bacterium, when created, is assigned a random "division threshold" denoted by m_n, which is the cumulative mass of substrate needed for the bacterium to divide. The m_n value is drawn at random from the uniform distribution on the interval ($0.9[(m_{avg})/(Y_{XS})]$, $1.1\ [(m_{avg})/(Y_{XS})]$) (10). Both m_n and the cumulative amount of substrate consumed by a bacterium to form biomass are stored in the *I* vector for that particular cell. Substrate consumption for each time increment is determined by multiplying (2-2) by the time step, Δt, and node volume, 27 μm^3. The cumulative amount of substrate consumed by the bacterium increases until it exceeds m_n, in which case the cell divides. Any excess substrate consumed (above m_n) is kept with the parent bacterium as part of a new m_n for future division. (After completing these simulation experiments, we revised this rule to split the excess substrate equally between the parent and daughter cells. Direct comparison indicates that due to the relatively small excess of substrate left after cellular division there is no difference in population growth between the two rules.)

The location (cube) of the newly created daughter cell is chosen at random from the 26 locations bordering the location of the mother cell (17 if the mother cell is on the substratum). If the selected cube is occupied, the daughter cell will displace cells in that direction until an empty cube is encountered. If the substratum or the original location

(due to the periodic boundary conditions) is reached before encountering an empty volume element, a different daughter cell location is chosen at random.

In BacLAB, detachment is entirely governed by the local concentration of the detachment factor. Let the parameter $C_{F,\max}$ denote a predetermined threshold concentration. Detachment occurs if and only if $C_F > C_{F,\max}$ at the cell's location or if a cell is no longer anchored to the substratum due to other cells detaching. Three different detachment rules were investigated in a computer experiment. The first presumes removal of any bacterium at each node point that has reached the detachment factor threshold, $C_{F,\max}$. This rule is referred to as local detachment. The second rule is similar to the first, but additionally removes any cell within a specified radius of detachment, R_d, of the node point where C_F exceeds $C_{F,\max}$. This rule attempts to account for degradation of the EPS matrix as described by (3). A hollowing of the biofilm structure is commonly observed with this detachment method, and it is therefore referred to as the hollow method. The third removal rule is similar to the second, with the exception that it also initiates the detachment of the plug or cylinder of biomass directly above the hollowed region. These detached particles typically resemble cylinders and, therefore, this method is referred to as the cylinder method.

Computational Steps

Figure 2-1 shows the algorithm that defines BacLAB. The numbered steps in Figure 2-1 correspond to this sequence of operations:

1. Initialize the carrier surface with N_c randomly placed spherical colonies of radius R_c. Each cell within the colonies is itself inoculated with a random amount of

substrate relative to division denoted by M, where M is chosen from a uniform (0, m_n) distribution.

2. Generate the substrate distribution for the current time step, t, by finding the steady state solution to (1).

3. Generate the detachment factor distribution for the current time step, t, by finding the steady state solution to (1).

4. For each cube in Γ, determine if it is occupied by a bacterium. If the cube is unoccupied, nothing further is done with that volume element at the current time step. If the cube is occupied, further calculations are performed.

5. Each bacterium consumes substrate based on (2) and the local concentration. The cumulative amount of substrate consumed for each cell, since its last division, is then updated.

6. Determine if C_F in the cube is above the detachment factor threshold, $C_{F,\max}$.

7. Remove the bacterium in the current cube and any additional bacteria in other cubes according the detachment rule specified. Additionally, identify and remove any floating clusters of bacteria.

8. Check if the bacterium has consumed enough substrate to divide.

9. Create a new bacterium neighboring the parent and leave excess substrate (not required for the creation of a daughter cell) with the parent bacterium according to the rules specified.

10. Move forward in time by Δt based on the events that occurred in steps 4–9.

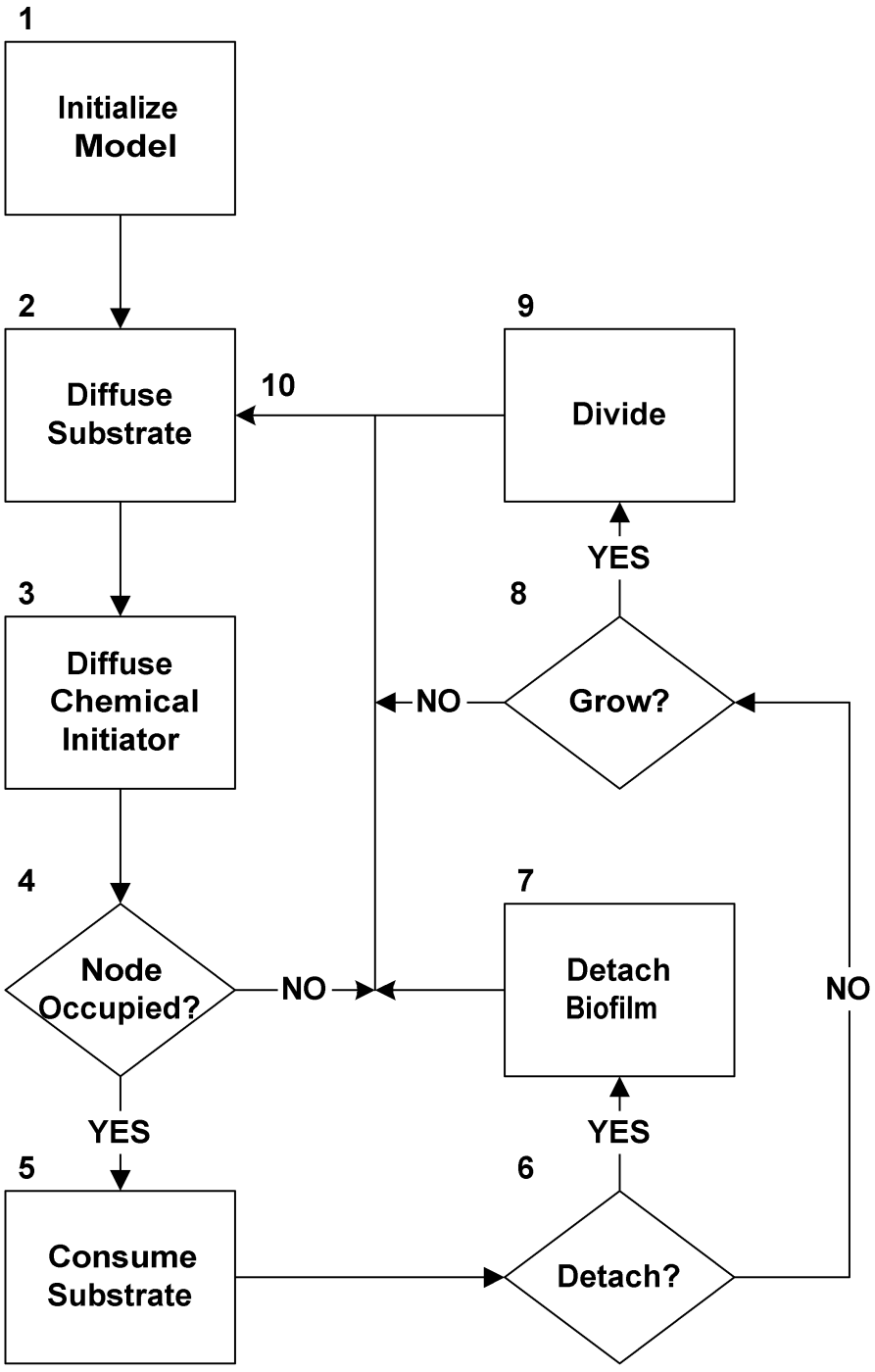

Figure 2-1. General procedure followed in a typical simulation using BacLAB

Computer Experiment

Methods

Twenty replicate simulations, each for 500 time steps, were conducted for each detachment rule. Table 2-1 shows the values used to model the kinetics and solute transport for a typical bacterial biofilm. These representative values fit the ranges available from the literature, with the exception of those pertaining to the detachment factor, which had to be assumed. Each of the computer simulations began by inoculating a 900μm x 900μm section of substratum with 28 randomly placed bacterial colonies (hemispheres) 30μm in diameter as shown in Figure 2a. With the concentration of the substrate in the bulk fluid fixed at 20 mg/l, the simulation evolved in accordance to the set of rules discussed in the Computational Steps section.

At each time step the program records the following response variables: cell areal density and biofilm thickness. Cell areal density is defined as the total number of cells in the model divided by the area and given as cell per unit area of substratum (typically cm^2). The biofilm thickness is defined as the maximum height obtained by any single bacterium within the simulation. Thickness was measured this way to emulate measurements obtained with an optical microscope where a slide is removed from a reactor and placed on the microscope stage (4). A 10X objective lens is then lowered until the top of the biofilm comes into focus and the fine adjustment dial setting is recorded. The objective is then lowered until the surface of the slide is in focus. The difference in the fine adjustment dial setting is then compared to a calibration curve to obtain the thickness.

Table 2-1. Nomenclature, and kinetic and diffusion parameters used in the simulations.

Parameter	Symbol	Value	Unit(s)
Spatial domain of the model	Γ		
Maximum specific growth rate	$\mu_{\max}$	0.3	h^{-1}
Time step	Δt	1.0	h
Identity pointer array	B		
Bulk detachment factor concentration	$C_{F,\text{bulk}}$	0.0	$g\ m^{-3}$
Detachment factor threshold	$C_{F,\max}$	$3.00 \cdot 10^{-3}$	$g\ m^{-3}$
Solute concentration	C_i		$g\ m^{-3}$
Bulk substrate concentration	$C_{S,\text{bulk}}$	20.0	$g\ m^{-3}$
Diffusivity of detachment factor in the aqueous phase (including the liquid, channels and voids)	$D_{F,\text{aq}}$	$2.09 \cdot 10^{-6}$	$m^2\ h^{-1}$
Relative effective diffusivity of detachment factor in biofilm	$D_{F,\text{e}} / D_{F,\text{aq}}$	0.3	
Diffusion coefficient of solute i	D_i		
Diffusion coefficient of solute i in aqueous phase	$D_{i,\text{aq}}$		
Relative effective diffusivity	$D_{i,\text{e}} / D_{i,\text{aq}}$		
Diffusivity of substrate in the aqueous phase (including the liquid, channels and voids)	$D_{S,\text{aq}}$	$2.52 \cdot 10^{-6}$	$m^2\ h^{-1}$
Relative effective diffusivity of substrate in biofilm	$D_{S,\text{e}} / D_{S,\text{aq}}$	0.45	
Detachment factor	F		
Bacterium information array	I		
Detachment factor production coefficient	k	0.5	h^{-1}
Monod half saturation coefficient	K_S	2.55	$g\ m^{-3}$
Volume element side length	L	3.00	μm
Average mass of an individual bacterium	m_{avg}	$1.00 \cdot 10^{-13}$	g
Mass needed for division	m_n		
Number of initial colonies	N_c	28	
Number of nodes in x-direction	N_x	300	
Number of nodes in y-direction	N_y	300	
Radius of initial colonies	R_c	15	μm
Radius of detachment	R_d	12	μm
Reaction rate of solute i	r_i		
Limiting substrate	S	Glucose	
Yield coefficient	Y_{XS}	0.45	$g_X\ g_S^{-1}$

Computational Resources

BacLAB was written in C++ and compiled using the GCC compiler collection available from the Free Software Foundation. The differential equation solver, pois3d, was obtained as Fortran source code which was compiled and linked to BacLAB, again with the GCC compiler collection.

All experiments were performed on a dual 800MHz Pentium III Mandrake Linux workstation with 1.5 gigabytes of PC133 SDRAM. A single experiment required approximately 700 megabytes of RAM. A simulation of 500 biofilm hours typically took about 8 computer hours. Although all experiments were conducted in a Linux/Unix environment, BacLAB has successfully been ported to a Microsoft Windows platform.

Analysis

The three-dimensional location data of each cell provides the ability to plot the biofilm in three-space and display the structural heterogeneity attained by BacLAB. Furthermore, by showing these images sequentially we are able animate the structural development of the biofilm.

To visualize important quantitive characteristics for each simulation, we plot the biofilm thickness and cell areal density as functions of time. The geometric mean cell count and mean biofilm thickness of the 20 simulations were plotted at each time step for all detachment rules. For each detachment rule, an 80% envelope was constructed by sorting the 20 simulation values at each time step and plotting the third smallest and third largest values. This envelope provides an upper and a lower bound between which 80% of our data lie.

To quantitively compare the different detachment rules, the mean log cell areal density and mean biofilm thickness for each simulation were calculated in the transition and the stationary phases, defined as 101-300 and 301-500 h, respectively. These times were chosen as oscillatory semi-steady values were observed after 300 h. Scatter plots of the means, log cell areal density versus thickness, were created to see whether the data were clustered according to the detachment rule. Paired sample t-tests were then conducted to compare means between detachment rules.

Results

Figures 2-2A-C demonstrate the structural heterogeneity obtainable in BacLAB. An animation showing the dynamics of the existing model is included as supplementary material with the online version of this paper at http://mic.sgmjournals.org. Figures 2-2A-C were created by extracting three frames from such an animation. The key feature in these plots is the degree of structural heterogeneity created by the chemically initiated detachment mechanisms alone, in the absence of bulk fluid shear.

Figures 2-3A-C present cell areal density data representing the 20 individual simulations for the local, hollow, and cylinder rules respectively, while figures 2-3D-F display the smoothed geometric mean and 80% envelope. Figure 2-4 displays the biofilm thickness data in a similar manner. Because each simulation describes the biofilm characteristics on a $0.0081 cm^2$ area of the surface, the areal cell density averaged over the 20 simulations corresponds to the areal density for a field of view of $0.162 cm^2$. The

variation among the 20 simulations shows that different areas of the biofilm are not synchronized, but can grow and detach at different times.

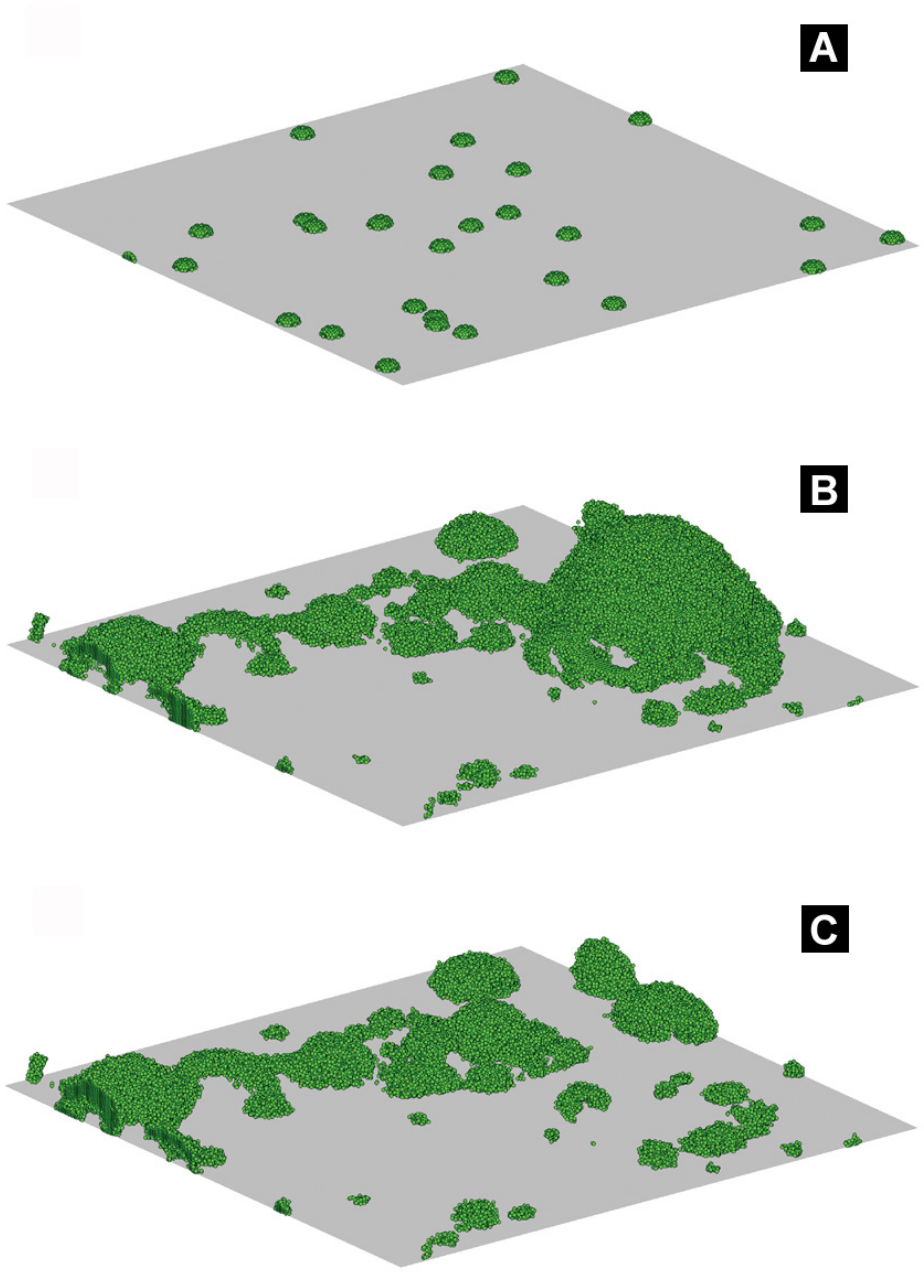

Figure 2-2. Computer simulated biofilm illustrating the biofilm (A) at the beginning of a simulation (Time t = 0), (B) prior to a detachment event, (t=330 h.), and (C) following detachment (t=335 h). Data for constructing the biofilm images were saved every fifth time step (at 5 h intervals).

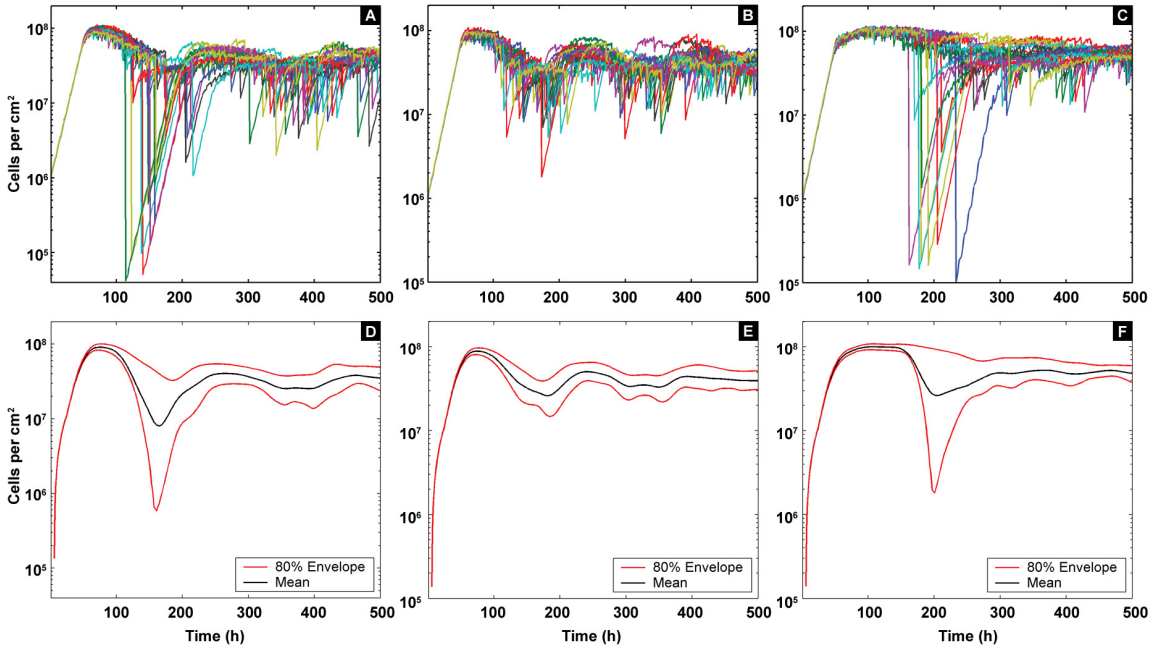

Figure 2-3. Time series of the cell areal density data representing the 20 individual simulations for the (A) local, (B) hollow, and (C) cylinder rules, respectively. Plots (D)-(F) show the smoothed geometric mean and 80% envelope for plots (A)-(C), respectively, using a LOWESS smoother with 1 iteration and 0.1 as the smoother span.

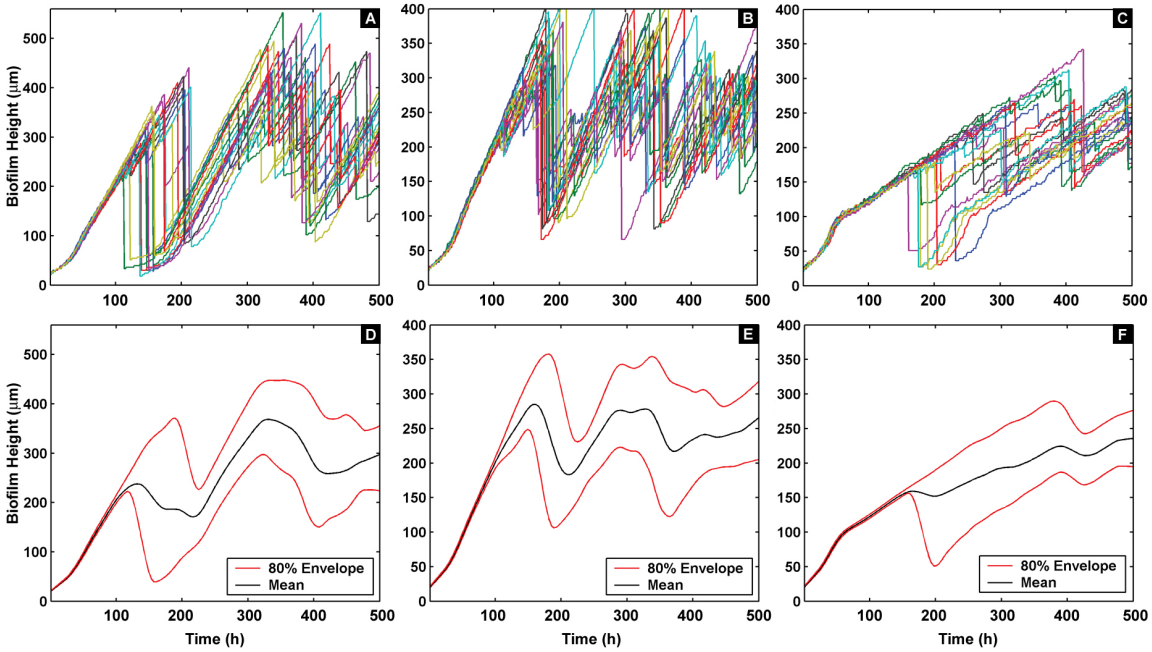

Figure 2-4. Time series of the biofilm thickness data representing the 20 individual simulations for the (A) local, (B) hollow, and (C) cylinder rules, respectively. Plots (D)-(F) show the smoothed arithmetic mean and 80% envelope for plots (A)-(C), respectively, using a LOWESS smoother with 1 iteration and 0.1 as the smoother span.

The cellular automata rules that govern the individual cells propagate into a consistent, but spatially variable, trend. The trends in Figures 2-3 and 2-4 are the exponential growth phase (0–100 h), followed by a relatively large sloughing event in the transition phase (101–300 h), followed by what appears to be an oscillatory "steady state" or stationary phase (301–500 h). These trends are observed for all three detachment rules to varying degrees. It should also be noted that the simulated cell areal densities are comparable to experimental densities found in the literature (12) for bacterial biofilms in general.

Figure 2-5 demonstrates how the data are clustered by detachment rule in a plot of log cell areal density verses biofilm thickness. Table 2-2 gives the mean and standard deviations of each characteristic for each detachment rule in the transition phase and stationary phase. All means within a given phase were statistically different $(\text{p-value} < 0.001)$ with the exception of the areal cell density assuming hollow and cylinder rules $(\text{p-value} = 0.036)$ and the biofilm thickness assuming local and hollow rules $(\text{p-value} = 0.052)$ in the transition phase. On the average, simulations with the local detachment rule result in a smaller areal cell density than does the hollow rule which is smaller than the cylinder rule. For thickness, the order is reversed with the thickness using the local rule greater than biofilms which follow the hollow rule which is greater than biofilms which follow the cylinder rule. Low areal density and high thickness suggest a spatially heterogeneous biofilm. Therefore, due to the negative relationship between areal density and biofilm thickness in our simulations, the local rule leads to the roughest biofilm while the cylinder rule leads to the smoothest.

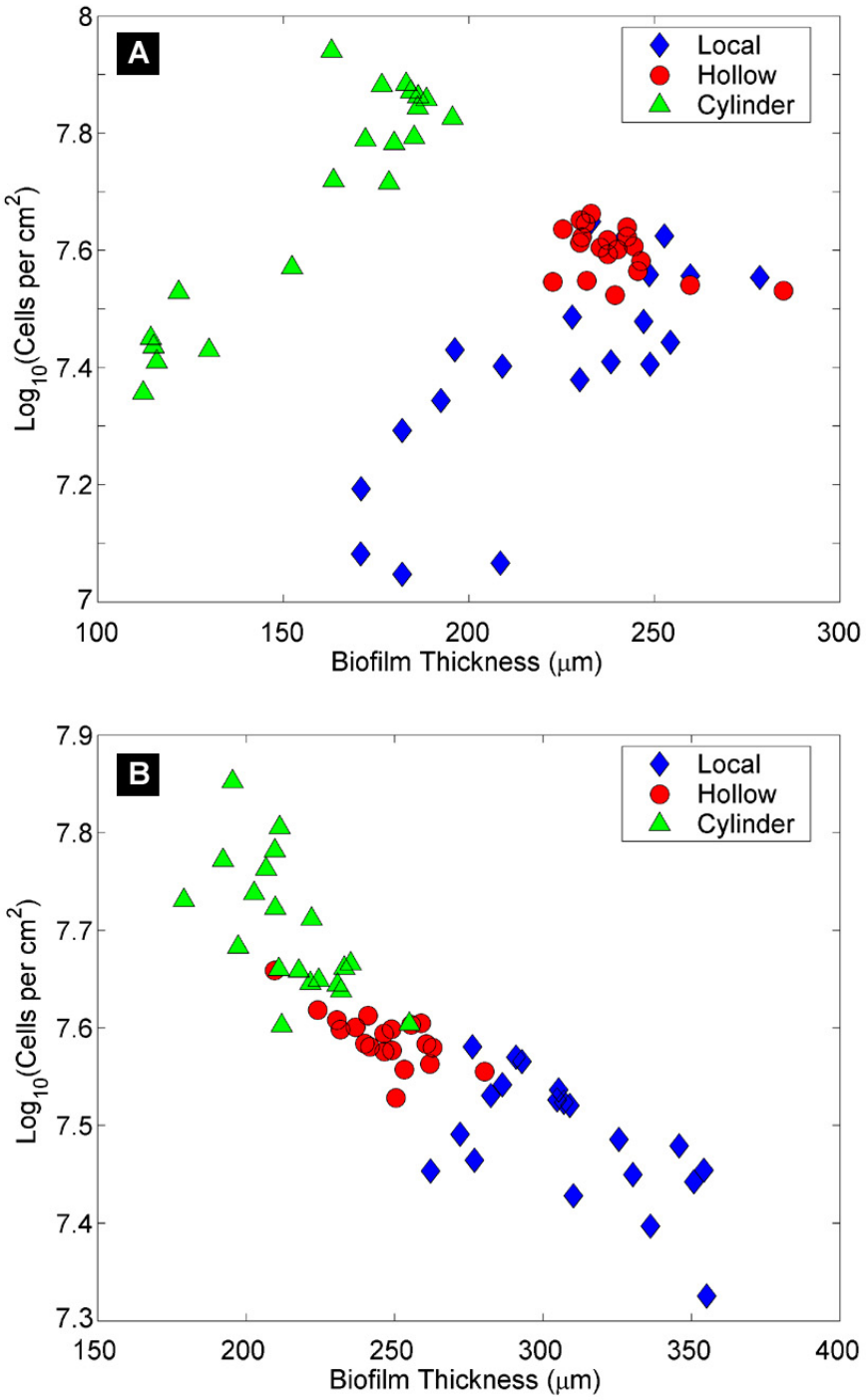

Figure 2-5. Cell areal density (geometric mean) and mean biofilm thickness for each simulation in scatter plots for the (A) transition and (B) stationary phase.

Table 2-2. Mean and standard deviation (SD) for the $\log_{10}$ areal cell density and for biofilm thickness data in the transition and stationary phases for each detachment rule.

Detachment Rule	**$\log_{10}$(cell areal density)**			
	Transition phase		**Stationary phase**	
	Mean	**SD**	**Mean**	**SD**
Local	7.4	0.18	7.4	0.06
Hollow	7.5	0.04	7.5	0.02
Cylinder	7.6	0.19	7.6	0.06
	Biofilm thickness			
	Transition phase		**Stationary phase**	
	Mean	**SD**	**Mean**	**SD**
Local	223	32.2	308	29.2
Hollow	239	13.6	246	15.6
Cylinder	160	30	215	17.6

Discussion

The goal of this research was to create a base model founded on well established transport equations that are easily adaptable to investigate conjectures at the biological level. The model does not incorporate all conventional biofilm development processes. Our model, BacLAB, controls biofilm development at the fundamental biofilm unit, the cell, and the resulting biofilm structure is produced by a process of self-organization. BacLAB with chemically induced detachment does create the typical heterogeneous "mushroom" shape observed experimentally in biofilms. While it is beyond the scope of this paper to investigate the detached particle size distribution, it is clear that BacLAB predicts detached clumps ranging in size from a few bacteria to near complete removal of the biofilm. At first blush this appears to agree with observations made by Stoodley et al. (24).

Modern biofilm research suggests that extracellular products play an important role in the development of biofilms. The BacLAB simulations assumed a chemical detachment factor accumulating locally leads to cellular detachment. Three rules were used to simulate the behavior of this chemically mediated detachment. While these detachment rules proved statistically different from one another, the differences are of little practical significance. The maximum difference in areal cell density between any two computer experiments in Figure 2-5 is less than a log. Furthermore, the difference in biofilm thickness is difficult to interpret because it is a measurement of the most extreme point and, as such, highly variable (see Figure 2-4). What we believe to be of practical significance is the observed trend (regardless of detachment rule) of a biofilm life cycle comparable to that observed in the laboratory. This life cycle begins when a carrier surface is inoculated with bacteria which undergo exponential growth until the biofilm reaches such a point that growth and detachment begin to offset one another. At this point the biofilm enters an oscillatory steady state where the biofilm is maintained as a heterogeneous entity by constant growth and periodic detachment. If the detachment rule is removed from BacLAB, the simulated biofilm grows as an ever thickening slab and no steady state is reached.

We have examined one reasonable, growth-related theoretical explanation to the process of biofilm development by assuming a detachment mechanism in systems that impose no shear-stress on the biofilm. Conceivably, a combination of shear and normal forces induced by flowing bulk liquid also contribute to biofilm detachment. It is perhaps more plausible that chemical mediation and bulk fluid force acting in concert are

responsible for the detachment of biofilms. The development of "mushroom" like biofilm clusters and interstitial voids and channels are typically thought to be a result of positive processes, like cell attachment, cell division and polymer production, and generally thought to result from some type of cellular organization. By refocusing on negative processes, such as cell detachment, we have shown that structures observed in real biofilms can be reproduced.

References

1. **Allison, D. G., H. S. J. D., W. L., H. J., and G. P.** 1999. Cellular detachment and dispersal from bacterial biofilms: A role for quorum sensing?, p. 279-286. *In* P. G. J. Wimpenny, J. Walker, M. Brading, and R. Bayston (ed.), Biofilms: The Good, The Bad and The Ugly. Bioline, Cardiff, UK.

2. **Barker, G. C., and M. J. Grimson.** 1993. A cellular automaton model of microbial growth. Binary **5:**132-137.

3. **Boyd, A., and A. M. Chakrabarty.** 1994. Role of alginate lyase in cell detachment of *Pseudomonas aeruginosa*. Appl. Environ. Microbiol. **60:**2355-2359.

4. **Characklis, W. G.** 1990. Laboratory Biofilm Reactors, p. 55-89. *In* W. G. Characklis and K. C. Marshall (ed.), Biofilms. John Wiley & Sons, inc., New York.

5. **Christensen, B. E., and W. G. Characklis.** 1990. Physical and chemical properties of biofilms, p. 93-130. *In* W. G. Characklis and K. C. Marshall (ed.), Biofilms. John Wiley & Sons, inc., New York.

6. **Colasanti, R. L.** 1992. Cellular automata models of microbial colonies. Binary **4:**191-193.

7. **Davies, D. G., M. R. Parsek, J. P. Pearson, B. H. Iglewski, J. W. Costerton, and E. P. Greenberg.** 1998. The involvement of cell-to-cell signals in the development of a bacterial biofilm. Science **280:**295-299.

8. **Eberl, H. J., C. Picioreanu, J. J. Heijnen, and M. C. M. van Loosdrecht.** 2000. A three-dimensional numerical study on the correlation of spatial structure, hydrodynamic conditions, and mass transfer and conversion in bioflms. Chem Eng Sci **55:**6209-6222.

9. **Ermentrout, G. B., and L. Edelstein-Keshet.** 1993. Cellular automata approaches to biological modeling. J Theor Biol **160:**97-133.

10. **Evens, M., N. Hastings, and B. Peacock.** 1993. Rectangular (uniform) continuous distribution, p. 137-140, Statistical Distributions. Wiley, New York.

11. **Hermanowicz, S. W.** 1998. A model of two-dimensional biofilm morphology. Wat. Sci. Tech. **37:**219-222.

12. **Jackson, G., H. Beyenal, W. M. Rees, and Z. Lewandowski.** 2001. Growing reproducible biofilms with respect to structure and viable cell counts. J. Microbiol. Meth. **47:**1-10.

13. **Kolter, R., and R. Losick.** 1998. One for all and all for one. Science **280:**226-227.

14. **Kreft, J. U., G. Booth, and J. W. T. Wimpenny.** 1998. BacSim, a simulator for individual-based modelling of bacterial colony growth. Microbiol. **144:**3275-3287.

15. **Monod, J.** 1949. The growth of bacterial cultures. Annu. Rev. Microbiol. **3:**371-394.

16. **Noguera, D. R., G. Pizarro, D. A. Stahl, and B. E. Rittmann.** 1999. Simulation of multispecies biofilm development in three dimensions. Wat. Sci. Tech. **39:**123-130.

17. **Picioreanu, C., M. C. M. van Loosdrecht, and J. J. Heijnen.** 1999. Discrete-differential modelling of biofilm structure. Wat. Sci. Tech. **39:**115-122.

18. **Picioreanu, C., M. C. M. van Loosdrecht, and J. J. Heijnen.** 1998. New combined differential-discrete cellular automaton approach for biofilm modeling: Application for growth in gel beads. Biotechnol. Bioeng. **57:**718-731.

19. **Potera, C.** 1999. Microbiology - Forging a link between biofilms and disease. Science **283:**1837-+.

20. **Rittmann, B. E., and J. A. Manem.** 1992. Development and experimental evaluation of a steady-state, multispecies biofilm model. Biotechnol. Bioeng. **39:**914-922.

21. **Rittmann, B. E., and P. L. McCarty.** 1980. Model of steady-state-biofilm kinetics. Biotechnol. Bioeng. **22:**2343-2357.

22. **Sauer, K., A. K. Camper, G. D. Ehrlich, J. W. Costerton, and D. G. Davies.** 2002. *Pseudomonas aeruginosa* displays multiple phenotypes during development as a biofilm. J. Bacteriol. **184:**1140-1154.

23. **Stewart, P. S., B. M. Peyton, W. J. Drury, and R. Murga.** 1993. Quantitative observations of heterogeneitis in *Pseudomonas aeruginosa* biofilms. (Notes). Appl. Environ. Microbiol. **59:**327-330.

24. **Stoodley, P., S. Wilson, L. Hall-Stoodley, J. D. Boyle, H. M. Lappin-Scott, and J. W. Costerton.** 2001. Growth and detachment of cell clusters from mature mixed-species biofilms. Appl. Environ. Microbiol. **67:**5608-5613.

25. **Wanner, O., and W. Gujer.** 1986. Multispecies biofilm model. Biotechnol. Bioeng. **28:**314-328.

26. **Wanner, O., and P. Reichert.** 1996. Mathematical modeling of mixed-culture biofilms. Biotechnol. Bioeng. **49:**172-184.

27. **Watnick, P., and R. Kolter.** 2000. Biofilm, city of microbes. J. Bacteriol. **182:**2675-2679.

28. **Wimpenny, J. W. T., and R. Colasanti.** 1997. A unifying hypothesis for the structure of microbial biofilms based on cellular automaton models. FEMS Microbiol. Ecol. **22:**1-16.

CHAPTER 3

THE ROLE OF NUTRIENT STARVATION IN BIOFILM DETACHMENT

The experimental work contained in this chapter was performed by other researchers at the Center for Biofilm Engineering. It is included here with the permission of those researchers to provide empirical support for the theoretical investigations of this dissertation.

Summary

A combination of experimental and theoretical approaches was used to investigate the role of nutrient starvation as a potential trigger for biofilm detachment. Experimental observations of detachment were made in a variety of biofilm systems using pure cultures of *Pseudomonas aeruginosa*. These observations indicated that biofilms grown under continuous flow conditions detached after flow was stopped, that hollow cell clusters were sometimes observed in biofilms grown in flow cells, and that lysed cells were apparent in the internal strata of colony biofilms. When biofilms were nutrient starved under continuous flow, detachment still occurred suggesting that starvation and not the accumulation of a signal molecule was responsible for triggering detachment in this particular system. A cellular automata computer model of biofilm dynamics was used to explore the starvation-dependent detachment mechanism. The model predicted biofilm structures and dynamics that were qualitatively similar to those observed experimentally. The predicted features included centrally located voids appearing in sufficiently large cell clusters, gradients in growth rate within these clusters, and release of most of the biofilm after simulating stopped-flow conditions. The model was also able to predict biofilm sloughing resulting solely from this detachment mechanism. These results support the

conjecture that nutrient starvation is an environmental cue for the release of microbes from a biofilm.

Introduction

The accumulation of microorganisms on surfaces to form biofilms is increasingly recognized as an important strategy of microbial survival in natural and engineered environments (6, 7). Biofilm accumulation is determined by the balance of attachment, growth, and detachment processes. Of these phenomena, the least understood is detachment. Detachment refers to the release of microbial cells, and their associated matrix polymers, from the biofilm to the bulk fluid bathing the film. Some of the factors that have been suggested to be important in biofilm detachment include matrix-degrading enzymes (1, 3, 13, 24), microbially-generated gas bubbles (14), nutrient levels and microbial growth status (2, 12, 15, 18-20), availability of multivalent cross-linking cations (2, 4, 23), fluid shear stress (15-17, 22), contact attrition (5), quorum-sensing signals (1, 9), and the activation of a lytic bacteriophage (26).

Some of these detachment mechanisms are purely physical, but others may be predominantly biological. Of the biological pathways to biofilm detachment, it is interesting to consider the possible triggers of the detachment process. What are the environmental cues that initiate the progression that eventually leads to the release of cells? Two possible triggers for detachment are embedded in the factors listed above. These are the accumulation of a metabolic product and the depletion of a metabolic substrate.

One intriguing mechanism of biofilm detachment invokes control by a quorum sensing signal. Dissolution of the biofilm matrix and release of bacteria is hypothesized to be triggered when the signal molecule, an excreted bacterial metabolite, accumulates to a threshold concentration. Such a mechanism leads directly to the prediction that natural signals or their analogues could be used to disperse biofilms and clean surfaces of biofouling (9). This mechanism of biofilm detachment was originally suggested by observations that arresting the flow of medium to a biofilm system caused the biofilm, within a few days, to spontaneously detach (8). Presumably the cessation of flow allows the detachment signal to accumulate, eventually reaching a concentration sufficient to trigger dispersion of the biofilm. The theoretical implications of this quorum sensing mechanism were investigated using a computer model (11). The model results indicated that high concentrations of the signal molecule excreted by bacteria occur in the center of cell clusters where diffusive egress is most restricted. This is same region in the biofilm that is nutrient deficient. This leads to an alternative explanation of biofilm detachment based on a starvation response.

The purpose of the work reported here was to investigate, through a combination of experimental and theoretical approaches, the role of nutrient starvation in biofilm detachment. We hypothesized that localized nutrient depletion in a biofilm induces starvation in some of the cells, and that these cells detach if the starvation persists for a sufficient period of time. Our investigation of this hypothesis employed two approaches. First, a cellular automata computer model of biofilm development was used to explore the behavior predicted by this detachment mechanism. Simulations from this model were compared to experimental observations of biofilm structure and detachment in

Pseudomonas aeruginosa biofilms grown in variety of biofilm reactors. The second approach was to perform laboratory experiments designed to discriminate the quorum-sensing hypothesis of biofilm detachment from the nutrient starvation hypothesis.

Materials and Methods

Experimental Methods

Three different systems were used to produce biofilms of *P. aeruginosa* strain PA01: drip-flow reactors, a glass capillary reactor, and colony biofilms. Biofilms were grown in continuous "drip-flow" reactors by flowing a minimal medium dropwise over inclined stainless steel coupons. The reactor system has been described elsewhere (21). The medium flow rate was 50 ml h^{-1}, the surface area of the coupons was 9.4 cm^2, and the temperature was 22°C. The medium (27) contained glucose, at 0.1 g/l, as the sole carbon and energy source. Biofilms were also grown in glass capillary tubes under continuous flow conditions as described previously (E. M. Werner, F. Roe, A. Bugnicourt, M. Franklin, A. Heydorn, S. Molin, B. Pitts, and P. S. Stewart, in press in Applied and Environmental Microbiology). The tube had a square cross section facilitating direct microscopic observation through the tube wall. The nominal inside dimension of the tube was 0.9 mm. The inoculum in this case was a PA01 strain carrying an inducible green fluorescent protein (GFP) (25). Biofilms were grown on one-tenth-strength tryptic soy broth at a flow rate of 20 ml h^{-1} for 24 h at 37°C. Biofilms were counterstained by injecting a solution of rhodamine B at 50 mg l^{-1} into the capillary to show the extent of the biomass, then examined by confocal scanning laser microscopy.

Colony biofilms were grown as described by Walters et al. (25). Colony biofilms were grown on tryptic soy agar for 48 h, then processed for transmission electron microscopy.

After four days of growth in a drip-flow reactor, biofilm detachment was stimulated by stopping flow of medium, laying the reactor flat, and covering the biofilm with 15 ml of medium to keep it hydrated. The system was left with no mixing for three days. Slides were then removed and allowed to drain to remove any detached cells from the biofilm and then scraped to enumerate attached bacteria. Detachment was also stimulated by subjecting four-day-old mature biofilms to glucose starvation by switching the influent to both the same medium lacking glucose and pure water. Slides were again removed and scraped to enumerate attached bacteria.

Analytical methods applied to biofilms grown as described above included enumeration of viable and total cells, determination of biofilm thickness, confocal scanning laser microscopy, and transmission electron microscopy. Viable cell numbers were determined by scraping biofilm from the coupons used in the drip-flow reactor, homogenization to disperse cell aggregates, serial dilution, and plating on R2A agar. Total cell numbers were determined by direct microscope enumeration of bacteria in the homogenate that had been deposited onto membranes by filtration. Biofilm thickness was determined by image analysis of DAPI-stained frozen sections (10). Biofilms in glass capillary tubes were examined with a Leica TCS NT scanning confocal laser microscopy. Excitation lines were at 488 nm and 568 nm, and emission was collected at 500-530 nm (green channel) and 585-615 (red channel). Transmission electron microscopy of colony biofilms was performed as described by Walters et al. (25).

Computational Methods

A full mathematical description of the model used in this study has been described elsewhere (11). As such, only a qualitative description of the model is presented here with modifications other than the detachment mechanism as follows: the limiting substrate was switched from glucose to oxygen, and the node spacing (volume element side length), L, was changed to 1.71 μm so as to correspond to an intrinsic cell density of 350 mg l^{-1}, volume of an individual cell of 0.5 μm^3, and a cell volume fraction of 0.1.

The bacterium level automata model, BacLAB, simulates the stochastic behavior of a bacterial biofilm on a submerged flat surface (substratum). BacLAB uses a hybrid modeling approach which linearly separates biofilm processes according to the natural time scales on which processes occur. A conventional deterministic differential equation approach is used in modeling chemical diffusion and reaction, while a stochastic cellular automata approach is used to model bacterial cell division, detachment, and movement.

To simulate detachment resulting from starvation, a mechanism consisting of two parameters was implemented into the BacLAB model: minimum local nutrient concentration, $C_{S,\min}$, and duration of time below that concentration, t_{detach}. When a bacterium's local nutrient concentration falls below $C_{S,\min}$, a counter for that bacterium records the cumulative number of time steps, Δt, during which the bacterium is exposed to the low nutrient condition. The counter begins at zero and continues until it reaches t_{detach} , at which point the cell detaches. If at any time step the local nutrient concentration for a bacterium rises above $C_{S,\min}$ the counter is decremented until it either returns to zero or the local nutrient concentration again falls below $C_{S,\min}$.

Each simulation begins by inoculating the substratum with N_c randomly placed spherical colonies of radius R_c. The algorithm that defines how BacLAB then proceeds is illustrated in Figure 3-1 with the numbered processes described as follows.

1. Differential Step – Diffusion of substrate from the bulk fluid into the biofilm.
2. CA Step – Perform the following operations on each volume element in the simulation.
    a. Determine if the volume element is occupied by a bacterium. If the volume element is unoccupied, nothing further is done with it for the current time step. If the volume element is occupied, more calculations are performed.
    b. Determine if the bacterium meets the requirements for detachment as described above.
    c. If requirement for detachment is satisfied, remove the bacterium from the simulation. Additionally, identify and remove any free floating bacteria in other volume elements that can no longer be traced back to the substratum as a result of the initial bacterium being removed.
    d. Allow the bacterium to consume substrate based on the local concentration of substrate, duration of the time step and the kinetics associated with the bacterium.
    e. Determine if the bacterium has consumed enough substrate to divide.
    f. Create a new bacterium neighboring the parent and split the excess substrate (not required for creation of the daughter cell) between the parent and daughter cells.

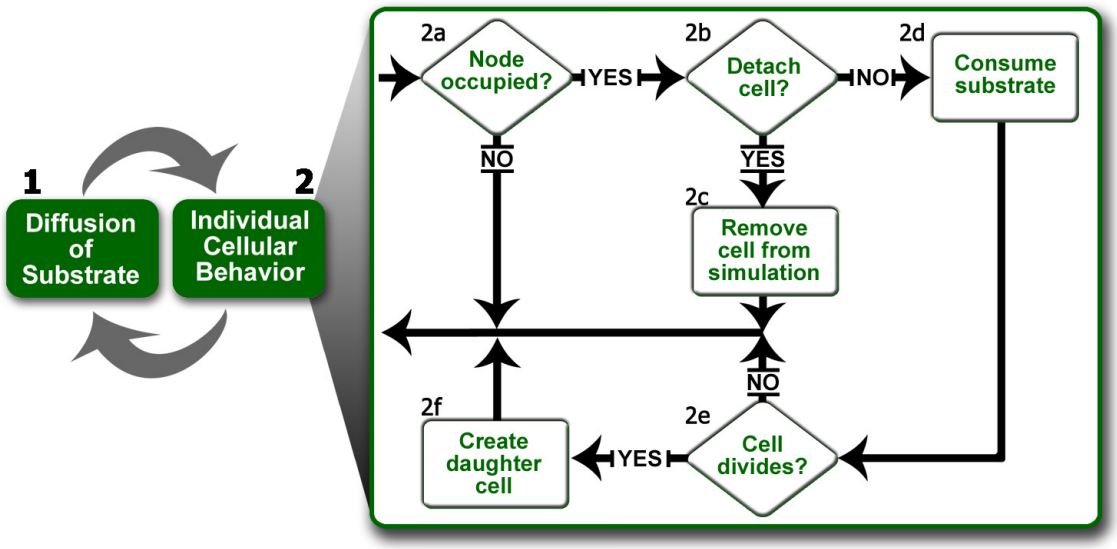

Figure 3-1. General procedure followed in a typical simulation using BacLAB. See the 'Computational Methods' section for an explanation of the sequence of operations.

Computer Experiment

To evaluate the effect of detachment resulting from starvation on biofilm development, we conducted ten replicate computer experiments simulating the starvation-induced detachment mechanism. Each experiment simulated 500 hours of biofilm development on a 512 x 512 μm rectangular surface according to the procedure outlined in Figure 3-1. Table 3-1 shows the values used to model the kinetics and solute transport for a typical biofilm. These representative values fit the ranges available from the literature, with the exception of those pertaining to detachment, for which no literature values are available.

Table 3-1. Kinetic and diffusion parameters used in the simulations

Parameter	Symbol	Value	Unit(s)
Maximum specific growth rate	μ_{max}	0.3	h^{-1}
Time step	Δt	1	h
Bulk substrate concentration	$C_{S,bulk}$	8	$g\ m^{-3}$
Diffusivity of substrate in the aqueous phase (including the liquid, channels and voids)	$D_{S,aq}$	$7.20 \cdot 10^{-6}$	$m^2\ h^{-1}$
Relative effective diffusivity of substrate in biofilm	$D_{S,e} / D_{S,aq}$	0.55	
Local nutrient concentration threshold	$C_{S,min}$	1	$g\ m^{-3}$
Monod half saturation coefficient	K_S	0.1	$g\ m^{-3}$
Volume element side length	L	1.71	μm
Average cell mass	m_{avg}	$1.75 \cdot 10^{-13}$	g
Number of initial colonies	N_c	28	
Number of nodes in x-direction	N_x	300	
Number of nodes in y-direction	N_y	300	
Radius of initial colonies	R_c	8.55	μm
Limiting substrate	S	Oxygen	
Duration of time below $C_{S,min}$ before detachment	t_{detach}	24	h
Yield coefficient	Y_{XS}	0.24	$g_X\ g_S^{-1}$

The computer model was also used to simulate a stop-flow experiment in which the nutrient concentration in the bulk water above the boundary layer was set to zero at a specified time step.

Computational Resources

BacLAB was written in C++ and compiled using the GCC complier collection (release 3.2.2) from the Free Software Foundation. All experiments were run on a dual AMD XP 2800+ workstation with 2 gigabytes of RAM. A single experiment typically required 24 computer hours to simulate 500 biofilm hours and utilized approximately 700 megabytes of RAM. These simulations took approximately 3 times longer than required for the quorum sensing mechanism simulations (11). The longer computation time is a

result of solving for solute concentrations iteratively on a finer time grid so as to avoid numerical artifacts in the critical regions where solute concentrations were nearly zero.

Results and Discussion

A combination of theoretical and experimental results bearing on the detachment of microorganisms from biofilms is presented below. The model simulations are not intended to provide quantitative matches to the experimental data. Rather, the simulations are offered as illustrations of general biofilm structures or behaviors that arise from starvation-dependent detachment. The agreement, or lack of agreement, between theory and experiment should be evaluated at a qualitative level.

Detachment from stopping the medium flow or omitting nutrients from the medium

After four days of growth in the drip-flow reactor, *P. aeruginosa* formed milky biofilms on the steel slides used as the attachment surface. The areal cell density at this stage of development was approximately 10^9 cells cm^{-2}. The $\log_{10}$ of the total cell areal density was 9.56 ± 0.13. The $\log_{10}$ of the viable cell areal density was 9.25 ± 0.21. The biofilms were approximately 300 microns thick. Biofilm detachment could be stimulated by stopping the flow of medium, laying the reactor flat, and covering the biofilm with 15 ml of medium to keep it hydrated. The system then rested, with no mixing at all, for three days. During this interval, the biofilm became increasingly translucent and the metal substratum progressively more visible. Slides were removed and scraped to enumerate attached bacteria. By both total cell counts and viable cell counts, stop-flow conditions produced at least a 1 log reduction in biofilm cell numbers (Table 3-2). This

means that more than 90% of the cells detached. To confirm this phenomenon, the number of cells in the fluid bathing the biofilm was also measured (Table3-3). These data show that the decrease in attached cells was accompanied by a concomitant and balancing increase in the number of free-floating cells.

Table 3-2. Detachment from P. aeruginosa biofilms. The error indicated is the standard deviation calculated for triplicate measurements.

Condition	Flow	Log_{10} Reduction Total Cells	Log_{10} Reduction Viable Cells
Flow Stopped	static	1.18 ± 0.30	1.21 ± 0.28
Glucose Omitted	shear	1.31 ± 0.16	1.02 ± 0.14
All Nutrients Omitted	shear	1.37 ± 0.18	1.36 ± 0.10

Table 3-3. Cell numbers in biofilm and planktonic phases before and after P. aeruginosa biofilm detachment. All values are the log10 of the cell number.

	Before Detachment			After Detachment		
Assay	Biofilm	Planktonic	Total	Biofilm	Planktonic	Total
Total Cells	10.6 ± 0.1	9.4 ± 0.1	10.7	9.7 ± 0.2	11.0 ± 0.4	11.0
Viable Cells	10.4 ± 0.2	9.4 ± 0.1	10.5	9.6 ± 0.2	10.5 ± 0.2	10.5

The time course of biofilm detachment after stopping medium flow in a drip-flow reactor is charted in Figure 3-2 along with the detachment predicted by BacLAB when simulating stop flow conditions. In both model and experiment, nearly 90% of the cells within a *P. aeruginosa* biofilm were lost during the first day. One difference between model and experiment is that the model predicted continued detachment whereas a tenacious layer of cells remain attached according to experimental data. Approximately 2 to 7% of the biofilm that was originally present remained for at least another 96 hours in the experiment. While the simulation correctly predicted the rapid release of most of the cells from the surface, it did not capture the long-term retention of a residual fraction of the cells.

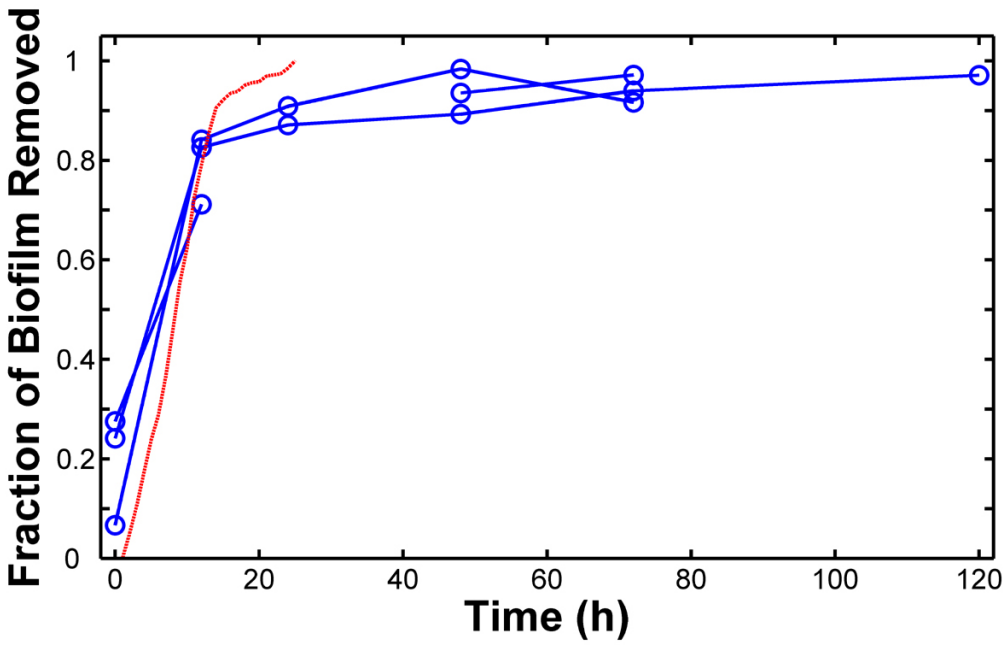

Figure 3-2. Biofilm detachment after stopping medium flow (a) in a drip-flow reactor (o) and as predicted by BacLAB (-) by averaging six simulations.

Detachment of biofilms in the drip-flow reactor system was visually confirmed by microscopic examination of frozen cross-sections. These observations were also consistent with loss of approximately 90% of the biofilm after stopping flow for three days. The biofilm thickness decreased from 334 ± 34 microns before detachment to 27 ± 10 microns after detachment.

While the preceding experimental data confirm the observation of biofilm detachment in response to cessation of medium flow, they do not tell us whether the detachment was a response to the accumulation of a signal molecule or if it was just a reaction to nutrient starvation. To probe this question, we subjected four-day-old mature biofilms to glucose starvation by switching the influent to the same medium lacking glucose. The continuing flow in these experiments should have prevented accumulation of a detachment signal. Furthermore, minimal synthesis of a detachment signal would be

expected in the absence of the sole carbon source. After three days of starvation under these continuous flow conditions, biofilms detached to a similar degree that they did in the static assay (Table 3-2). The same result was also obtained when pure water was used during the starvation period in place of glucose-free medium. These data support the hypothesis that biofilm detachment is a response to nutrient depletion and not the accumulation of a signal molecule, at least in this particular system.

Observation and prediction of hollowing of biofilm cell clusters

When *P. aeruginosa* biofilms were grown in continuous flow capillary reactors, hollow cell clusters were sometimes observed using confocal scanning laser microscopy (Figure 3-3). The hollowing appeared to be spatially organized with two key features: 1) hollowing only occurred in cell clusters that had reached a sufficient size, and 2) voids were always centrally located at the substratum. These features are qualitatively consistent with the conjecture that detachment depends on nutrient availability.

Simulation results from BacLAB predicted biofilm cell cluster hollowing with the same features. Hollowing occurred at the substratum in the center of larger clusters (Figure 3-4A). The hollow regions in the biofilm corresponded to areas of low nutrient concentration (Figure 3-4B). The model predicted that cells near the bulk fluid interface were growing much more rapidly than those cells deeper in the biofilm (Figure 3-4C). The simulations indicated that the transition from high to low growth rate was spatially sharp, occurring over a distance of a few tens of microns at most (Figure 3-4C).

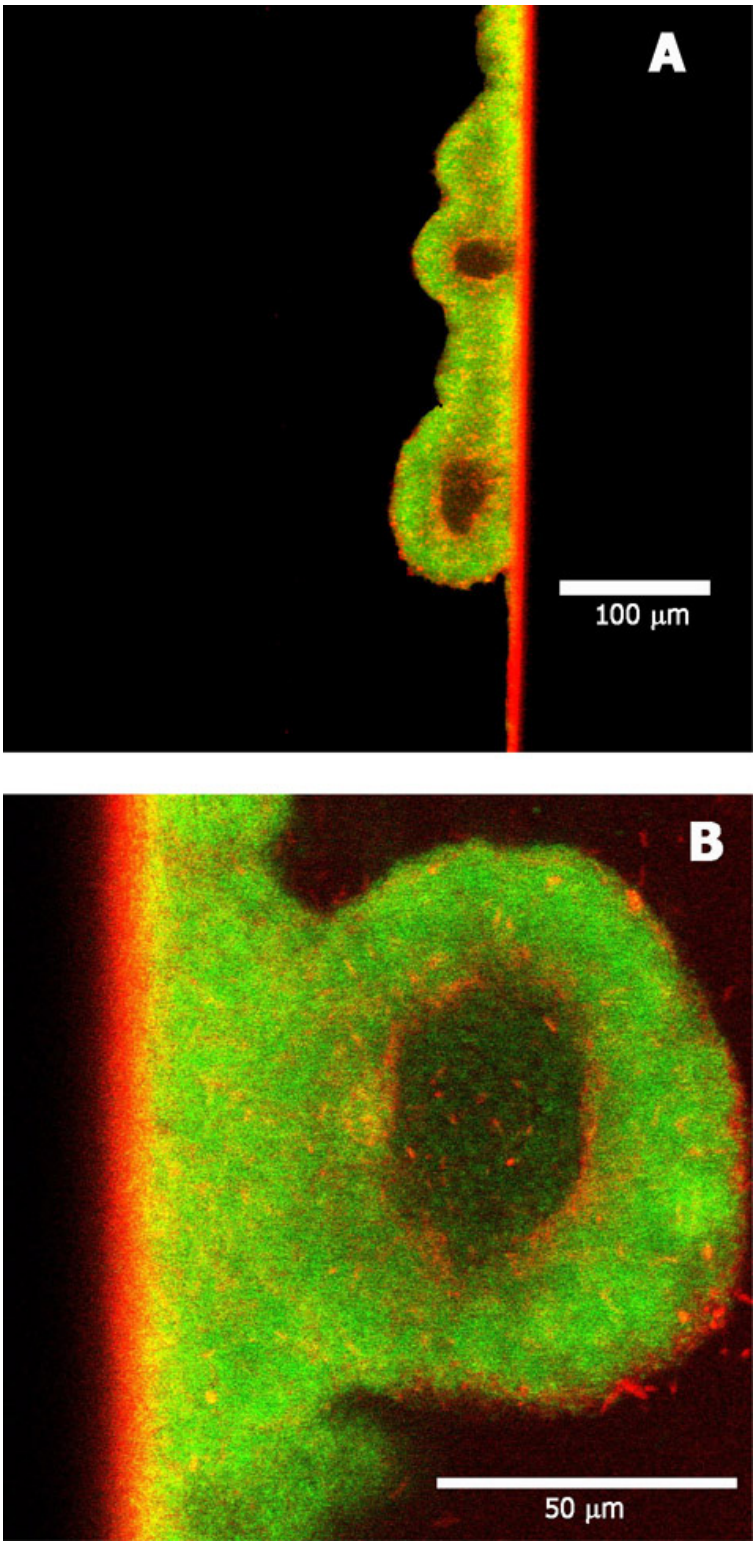

Figure 3-3. Confocal scanning laser microscopy of hollow P. aeruginosa biofilm clusters. Biofilms were grown in a glass capillary tube under continuous flow. The distribution of active cells is revealed by a GFP (green) and the extent of biomass by the rhodamine B counterstain (red).

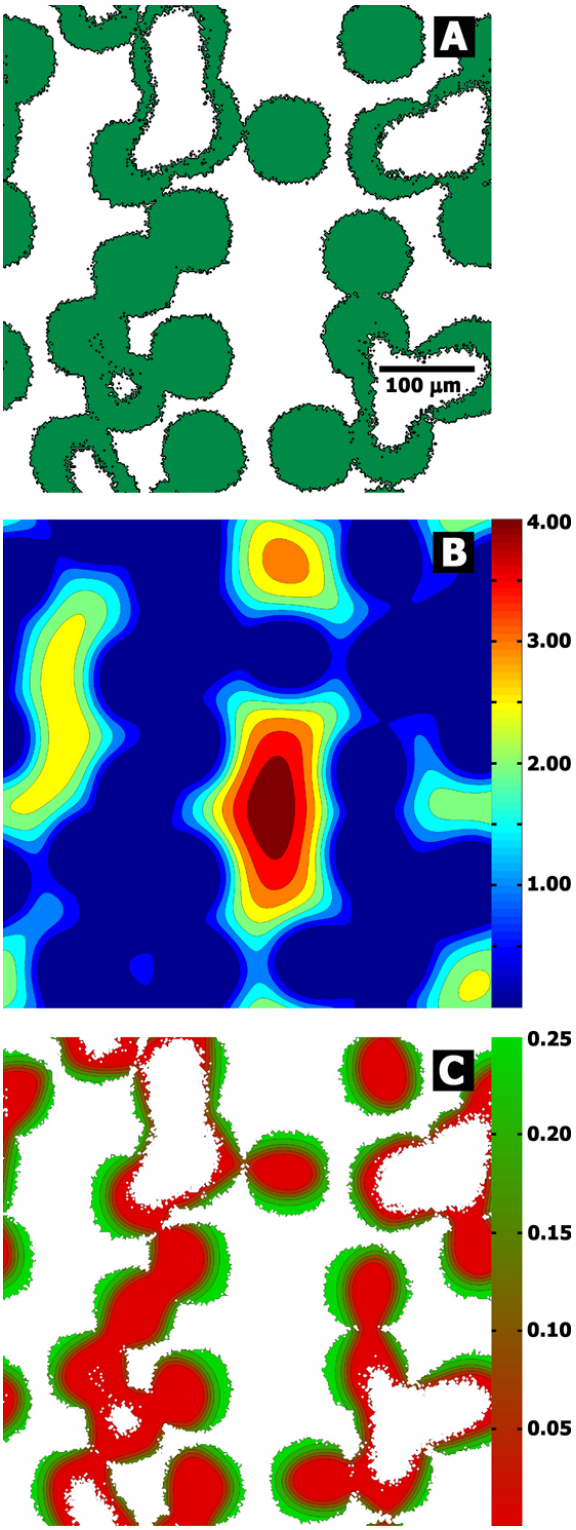

Figure 3-4. Representative simulation in BacLAB predicting hollow biofilm cell clusters. The distribution of biomass (A) at the substratum suggests that larger clusters develop hollow interiors. Also shown are the predicted distributions of oxygen (B) at the substratum and the specific growth rate (C) at the substratum.

The presence of voids within biofilm cell clusters was reinforced by microscopic observation of rapid motility of bacterial cells inside some cell clusters. (A movie of seething within a *P. aeruginosa* biofilm cluster can be viewed at http://www.erc.montana.edu/Res-Lib99-SW/pubs/Theses/Database/TD_DisplayScript.asp.) The rapid motion of these cells suggests that the local viscosity in the cluster interior has been reduced. To achieve such a reduction in viscosity, most of the cell mass and extracellular matrix material in the cluster void would have to have been degraded or released to the bulk fluid.

Webb et al. (26) and Purevdorj-Gage and Stoodley (L. B. Purevdorj-Gage and P. Stoodley, submitted for publication) have observed hollowing of *P. aeruginosa* biofilm cell clusters similar to that described here. Webb et al. have also presented strong evidence that this behavior was associated with the activation of a bacteriophage (26). This suggests the following mechanism of hollowing in these biofilms. At a certain stage of biofilm development, the phage is activated in the center of some cell clusters. The phage causes some, but not all, cells to lyse. Enzymes possibly including polysaccharide lyases, proteases, or nucleases, are released and locally thin the EPS matrix. Some of the cells survive the phage and are either released through a pore to the bulk fluid or are trapped inside the void where they become motile and seethe inside the hollow cluster. The hollowing that is observed would, according to this hypothesis, result from a combination of cell lysis, EPS degradation, and cell dispersal. In support of the role for cell lysis, we have observed lysis in the internal strata of *P. aeruginosa* colony biofilms (Figure 3-5).

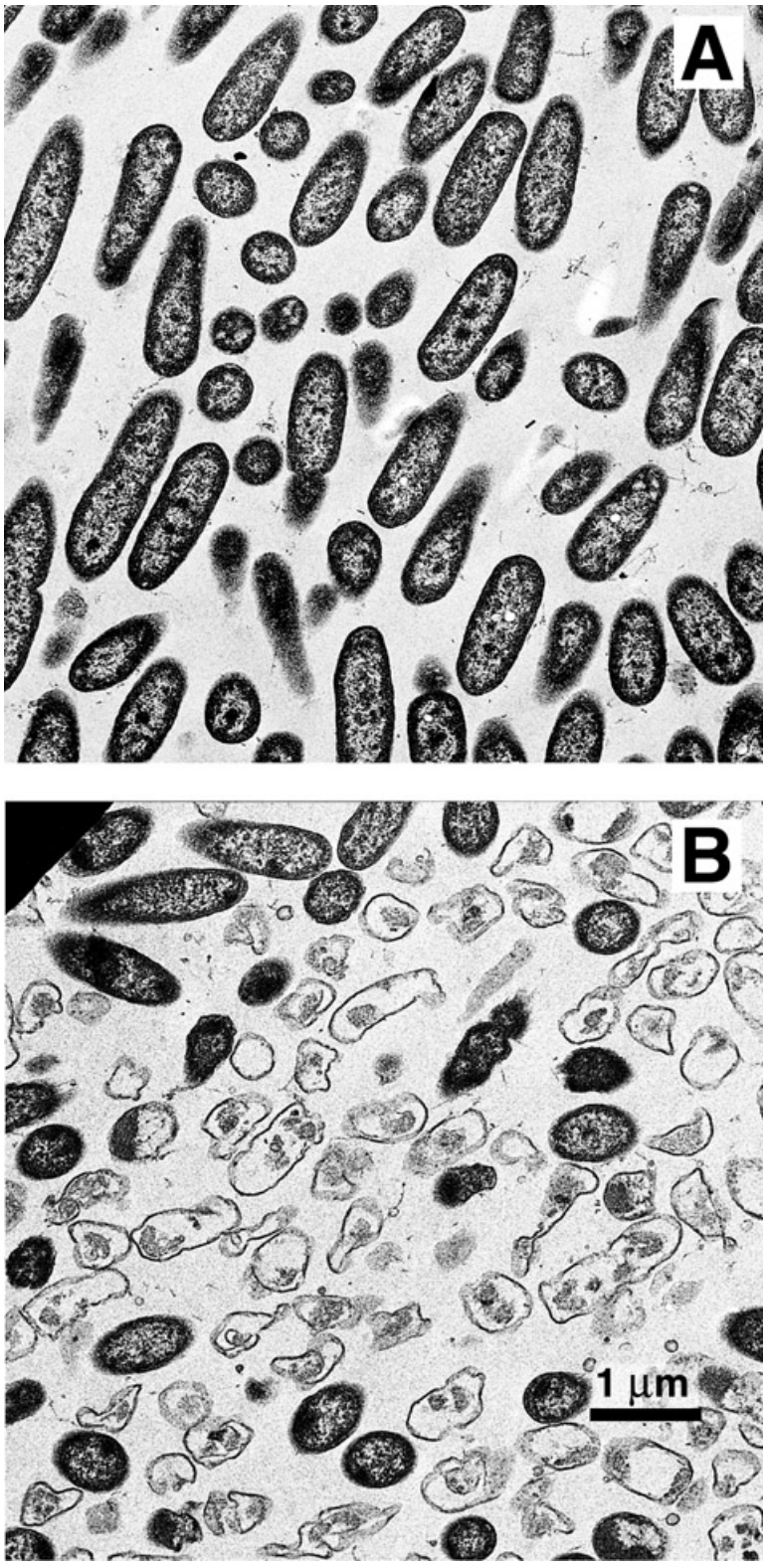

Figure 3-5. Transmission electron microscopic observation of cell lysis in the interior of P. aeruginosa colony biofilms (B). Little lysis is evident in cells near the air interface of the biofilm (A).

We propose that the activation of the phage in these biofilms is a consequence of prolonged nutrient starvation. In other words, nutrient starvation is the trigger for this detachment process. Computer model simulations of biofilm development based on a conjecture of starvation-dependent detachment generate biofilm structures that resemble those observed in experiments. This mechanism can explain the detachment that is observed when medium flow is stopped. The simulations are also consistent with the widespread, if anecdotal, observation of biofilm sloughing, a phenomenon that other models of biofilm detachment fail to capture. Experiments with biofilms grown in the drip-flow reactor system support the nutrient-starvation detachment hypothesis and are inconsistent with the signal-mediated detachment hypothesis.

An alternative explanation is simply that natural hydrolytic processes cause degradation of the biofilm matrix unless there is ongoing synthesis of new matrix material. Under nutrient starvation conditions, biofilms detach because the slow breakdown of extracellular polymeric substances is not compensated for by new matrix production. Thus, bacteria ensure their eventual release from a biofilm by producing enzymes capable of degrading biofilm matrix polymers. These enzymes, which might be proteases, polysaccharide lyases, or nucleases, are conceived to be continually secreted by growing cells during formation of the biofilm. Such enzymes may be tethered to the cell or to matrix polymers to retain them in the biofilm. These lytic enzymes catalyze slow hydrolysis of the biofilm matrix, independent of the metabolic state of the cell from whence they originated. In the growing biofilm, this ongoing degradation is balanced or compensated for by the active synthesis of new matrix polymers. In an environment that becomes nutrient-limited, or in starved regions of a biofilm, the steady degradation of

matrix polymers precedes while no new synthesis occurs. This leads to weakening of the biofilm matrix and eventually to the detachment of bacteria and associated matrix material. This is a passive mechanism of detachment that can be implemented even if nutrients are lacking or if antimicrobial agents are present. This mechanism of detachment is consistent with some previous reports (1, 6, 19).

Prediction of biofilm sloughing

An interesting observation from the BacLAB simulations was the prediction of sloughing. In the early stages of biofilm development, clusters developed hollowed interiors through lysis and detachment as previously described. The remaining biomass then appeared as "mushrooms" or large chunks of biofilm loosely tethered to the substratum. The few bacteria anchoring the biofilm at some point became nutrient starved and detached, releasing large chunks of biomass back into the bulk fluid (Figure 3-6).

Biofilm sloughing occurred regularly in BacLAB simulations. Of the ten replicate simulations conducted, six had sloughing events that resulted in a loss of 50% or more of the biomass (> 0.301 $\log_{10}$ reduction) in one time step (Figure 3-7). Smaller detachment events, releasing multicellular aggregates, occurred continually, offsetting the ongoing growth of biofilm cells and allowing the biofilm to reach an oscillatory steady. While it was beyond the scope of this work to investigate the detached particle size distribution, it is clear that detachment resulting from nutrient starvation would be expected to lead to the release of everything from single cells to nearly 70% of the biofilm biomass in a single event.

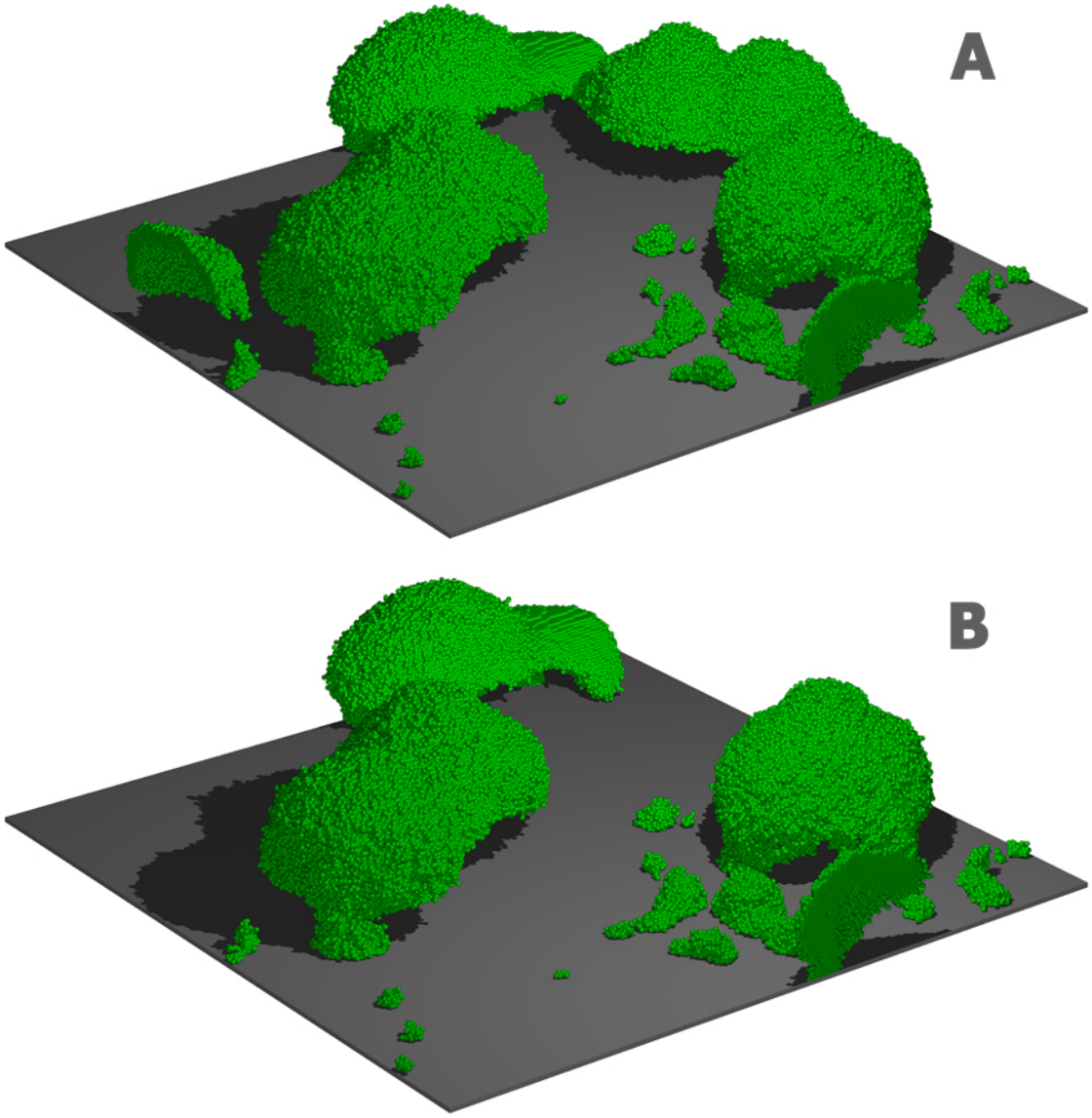

Figure 3-6. BacLAB simulation showing biofilm sloughing. The biofilm structure at 235 h, prior to the sloughing event, and at 240 h, after the sloughing event. (The entire simulation can be viewed at http://www.erc.montana.edu/Res-Lib99-SW/pubs/Theses/Database/TD_DisplayScript.asp.)

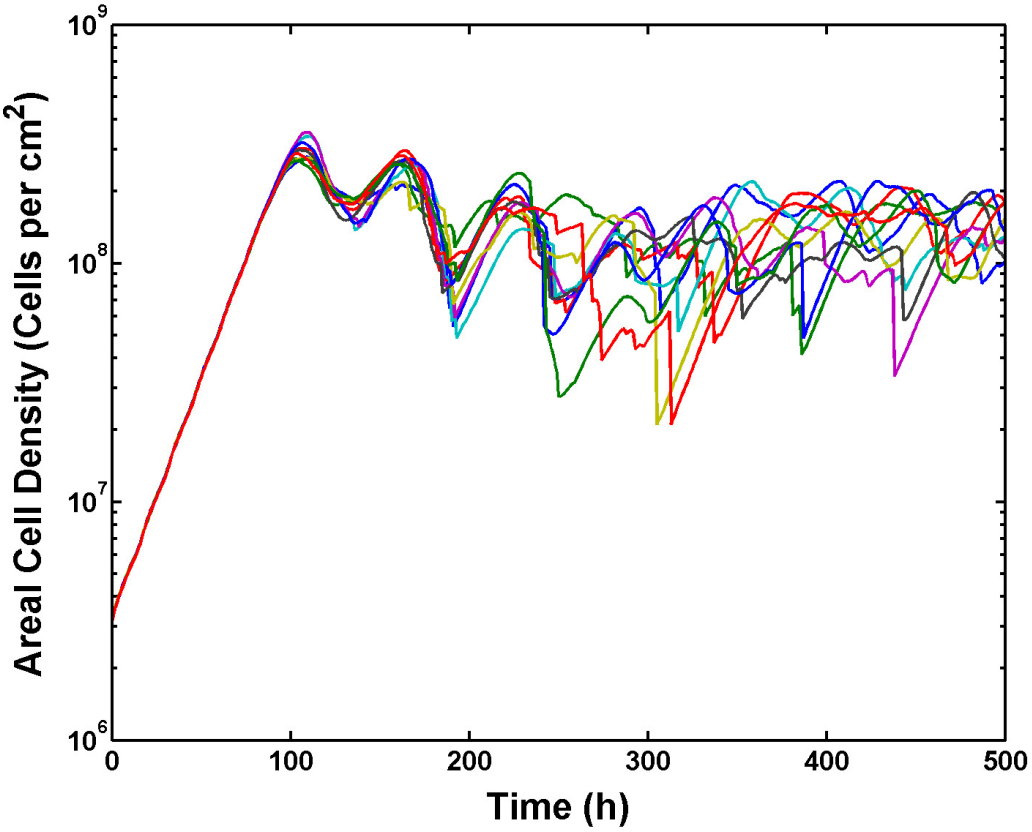

Figure 3-7. BacLAB replicate simulations showing sloughing as revealed by sharp decreases in areal cell density. The parameter settings were identical in these 10 simulations; only the random initial distribution of cells on the substratum differed in the ten runs. Sloughing events, defined as a loss of 50% of biofilm biomass in a single time step (1 h) occurred in 6 of the 10 simulations.

Surely there are multiple pathways to biofilm detachment – simple physical shearing by fluid flow, cell lysis, and enzymatic dissolution of matrix material. Detachment is a critical process governing biofilm structure and the rate and extent of biofilm accumulation. It regulates the dissemination of microorganisms from a contaminated surface. Yet almost nothing is known about biofilm detachment because this phenomenon cannot be studied by conventional microbial methods. New experimental and computational studies are needed to understand and isolate the factors that control biofilm detachment.

References

1. **Allison, D. G., B. Ruiz, C. SanJose, A. Jaspe, and P. Gilbert.** 1998. Extracellular products as mediators of the formation and detachment of Pseudomonas fluorescens biofilms. FEMS Microbiol. Lett. **167:**179-184.

2. **Applegate, D. H., and J. D. Bryers.** 1991. Effects of carbon and oxygen limitations and calcium concentrations on biofilm removal processes. Biotechnol. Bioeng. **37:**17-25.

3. **Boyd, A., and A. M. Chakrabarty.** 1994. Role of alginate lyase in cell detachment of *Pseudomonas aeruginosa*. Appl. Environ. Microbiol. **60:**2355-2359.

4. **Caccavo, F., B. Frolund, F. V. Kloeke, and P. H. Nielsen.** 1996. Deflocculation of activated sludge by the dissimilatory Fe(III)-reducing bacterium Shewanella alga BrY. Appl. Environ. Microbiol. **62:**1487-1490.

5. **Chang, H. T., B. E. Rittmann, D. Amar, R. Heim, O. Ehlinger, and Y. Lesty.** 1991. Biofilm detachment mechanisms in a liquid-fluidized bed. Biotechnol. Bioeng. **38:**499-506.

6. **Costerton, J. W., Z. Lewandowski, D. E. Caldwell, D. R. Korber, and H. M. Lappin-Scott.** 1995. Microbial biofilms. Annu. Rev. Microbiol. **49:**711-745.

7. **Costerton, J. W., and P. S. Stewart.** 2001. Battling biofilms. Scientific American **285:**74-81.

8. **Davies, D. G., M. R. Parsek, J. P. Pearson, B. H. Iglewski, J. W. Costerton, and E. P. Greenberg.** 1998. The involvement of cell-to-cell signals in the development of a bacterial biofilm. Science **280:**295-299.

9. **Hentzer, M., K. Riedel, T. B. Rasmussen, A. Heydorn, J. B. Andersen, M. R. Parsek, S. A. Rice, L. Eberl, S. Molin, N. Hoiby, S. Kjelleberg, and M. Givskov.** 2002. Inhibition of quorum sensing in *Pseudomonas aeruginosa* biofilm bacteria by a halogenated furanone compound. Microbiol. **148:**87-102.

10. **Huang, C.-T., P. S. Stewart, and G. A. McFeters.** 1998. The study of microbial biofilms by classical fluorescence microscopy. *In* M. H. F. Wilkinson and F. Schut (ed.), Digital Image Analysis of Microbes: Imaging, Morphometry, Fluorometry and Motility Techniques and Applications. John Wiley & Sons.

11. **Hunt, S. M., M. A. Hamilton, J. T. Sears, G. Harkin, and J. Reno.** 2003. A computer investigation of chemically mediated detachment in bacterial biofilms. Microbiol. **149:**1155-63.

12. **Jackson, D. W., K. Suzuki, L. Oakford, J. W. Simecka, M. E. Hart, and T. Romeo.** 2002. Biofilm formation and dispersal under the influence of the global regulator CsrA of *Escherichia coli*. J. Bacteriol. **184:**290-301.

13. **Kaplan, J. B., C. Ragunath, N. Ramasubbu, and D. H. Fine.** 2003. Detachment of *Actinobacillus actinomycetemcomitans* biofilm cells by an endogenous {beta}-hexosaminidase activity. J. Bacteriol. **185:**4693-4698.

14. **Ohashi, A., and H. Harada.** 1994. Characterization of detachment mode of biofilm developed in an attached-growth reactor. Wat. Sci. Tech. **30:**35-45.

15. **Peyton, B. M., and W. G. Characklis.** 1993. Statistical analysis of the effect of substrate utilization and shear stress on the kinetics of biofilm detachment. Biotechnol. Bioeng. **41:**728-735.

16. **Picioreanu, C., M. C. M. van Loosdrecht, and J. J. Heijnen.** 2001. Two-dimensional model of biofilm detachment caused by internal stress from liquid flow. Biotechnol. Bioeng. **72:**205-218.

17. **Rittmann, B. E.** 1982. The effect of shear stress on biofilm loss rate. Biotechnol. Bioeng. **24:**501-506.

18. **Sawyer, L. K., and S. W. Hermanowicz.** 1998. Detachment of biofilm bacteria due to variations in nutrient supply. Wat. Sci. Tech. **37:**211-214.

19. **Speitel, G. E., and F. A. Digiano.** 1987. Biofilm shearing under dynamic conditions. J. Environ. Eng. ASCE **113:**464-475.

20. **Stewart, P. S.** 1993. Model of biofilm detachment. Biotechnol. Bioeng. **41:**111-117.

21. **Stewart, P. S., J. Rayner, F. Roe, and W. M. Rees.** 2001. Biofilm penetration and disinfection efficacy of alkaline hypochlorite and chlorosulfamates. J. Appl. Microbiol. **91:**525-32.

22. **Stoodley, P., S. Wilson, L. Hall-Stoodley, J. D. Boyle, H. M. Lappin-Scott, and J. W. Costerton.** 2001. Growth and detachment of cell clusters from mature mixed-species biofilms. Appl. Environ. Microbiol. **67:**5608-5613.

23. **Turakhia, M. H., K. E. Cooksey, and W. G. Characklis.** 1983. Influence of a calcium-specific chelant on biofilm removal. Appl. Environ. Microbiol. **46:**1236-1238.

24. **Vats, N., and S. F. Lee.** 2000. Active detachment of *Streptococcus mutans* cells adhered to epon-hydroxylapatite surfaces coated with salivary proteins in vitro. Arch. Oral. Biol. **45:**305-314.

25. **Walters, M. C., 3rd, F. Roe, A. Bugnicourt, M. J. Franklin, and P. S. Stewart.** 2003. Contributions of antibiotic penetration, oxygen limitation, and low metabolic activity to tolerance of *Pseudomonas aeruginosa* biofilms to ciprofloxacin and tobramycin. Antimicrob. Agents Chemother. **47:**317-23.

26. **Webb, J. S., L. S. Thompson, S. James, T. Charlton, T. Tolker-Nielsen, B. Koch, M. Givskov, and S. Kjelleberg.** 2003. Cell death in *Pseudomonas aeruginosa* biofilm development. J. Bacteriol. **185:**4585-92.

27. **Wentland, E. J., P. S. Stewart, C. T. Huang, and G. A. McFeters.** 1996. Spatial variations in growth rate within *Klebsiella pneumoniae* colonies and biofilm. Biotechnol. Progr. **12:**316-321.

CHAPTER 4

SIMULATION OF PROTECTION FROM KILLING BY ANTIMICROBIAL AGENTS USING A THREE-DIMENSIONAL BIOFILM MODEL

Summary

A three-dimensional cellular automata model of biofilm dynamics was adapted to simulate the protection from killing by antimicrobial agents afforded to microorganisms in the biofilm state. The model incorporated diffusion and simultaneous utilization of a single substrate, growth and displacement of cells, detachment, and killing by an antimicrobial agent. The rate of killing was assumed to be directly proportional to the local concentration of substrate available to the microorganisms. To justify the assumption that the antimicrobial agent penetrated the biofilm rapidly, the transient diffusion of an antimicrobial agent into the biofilm was computed. The time required to attain 90 percent of the dosed antimicrobial agent concentration throughout every point in the biofilm was calculated to be bounded between 15 and 159 s. This delay was judged to be insignificant in comparison to the 12 h antimicrobial agent dose duration and was therefore neglected in subsequent model runs. Some of the features predicted by this model included development of dynamic, heterogeneous biofilm structures, gradients in substrate concentration leading to regions of substrate depletion in the interior of large cell clusters, variable killing by an antimicrobial agent from one simulation to the next, greater killing of cells at the periphery of cell clusters compared to those cells which were more deeply embedded, and reduced overall antimicrobial susceptibility of cells in the biofilm. The log reduction computed for the biofilm ranged from 0.34 to 1.59 for a 12 h

antimicrobial exposure, whereas a 4.44 log reduction for free-floating cells in the bulk fluid would be expected for the same treatment. Extended antimicrobial doses predicted eradication of all living cells from the biofilm in approximately 44 h. These simulations show that substrate limitation can contribute to the protection from antimicrobial agents in biofilms but cannot explain the long-term persistence of biofilm viability that is often observed in practice.

Introduction

Microorganisms within biofilms have a remarkable tolerance to killing by antimicrobial agents (8, 9, 16). The reduced susceptibility of bacteria and yeast in biofilms is recognized as an important factor in the persistence of some chronic infections and the troublesome recurrence of fouling in industrial systems. The protective mechanisms behind antimicrobial tolerance in biofilms are only moderately understood but may involve poor antimicrobial penetration, physiological heterogeneity in the biofilm population, deployment of adaptive stress responses, expression of biofilm-specific genes, and the presence of phenotypic variants or persister cells (4, 8, 15). It seems likely that a combination of these factors determines the overall protection in the biofilm (2, 8, 15, 16).

Computer models of biofilm dynamics complement experimental investigations and thus are valuable tools in the exploration of biofilm phenomena. One of the ways that models can be used is to test conjectures or make predictions about how specific processes affect biofilm structure or function. Theoretical explorations are particularly attractive because often there are multiple mechanisms at work which are difficult to

separate experimentally. We have been interested in using biofilm models to explore the degree of protection from killing by antimicrobials that can be realized by specific tolerance mechanisms. A handful of previous studies have described biofilm models that incorporate antimicrobial action (10, 14, 17).

Two longstanding explanations for the reduced susceptibility to antimicrobials are poor penetration of the antimicrobial into the biofilm and substrate limitation leading to slow growth. There are a handful of papers describing neutralization of an antimicrobial agent by a reaction as it diffuses into the biofilm (1, 5, 18). However, antimicrobial agents that do not react or bind with the biofilm can be expected to penetrate over a matter of seconds or minutes (13). Examples of several antimicrobial agents that penetrate biofilms without killing microorganisms at the observed rate of their planktonic counterparts are plentiful (1, 3, 6, 11, 19, 23). This suggests that some other mechanism is providing protection from the antimicrobial agents.

The possibility of substrate limitation leading to inactive, and less susceptible cells, remains an attractive explanation for the recalcitrance of biofilm cells to antimicrobial agents. It is now clear that gradients in substrate concentrations exist within biofilms (5). These concentration gradients give rise to corresponding gradients in microbial growth rate and activity as observed by researchers using fluorescent probes and reporter genes (12, 20, 21). Since antimicrobials are thought to be more effective in killing actively growing cells, it seems reasonable that in substrate limited regions of a biofilm, microorganisms could better tolerate the presence of an antimicrobial agent by virtue of their inactivity. However, one would expect that as growing cells within the biofilm are killed, substrate would penetrate into regions that were previously substrate

depleted. Thus, microorganisms that were previously dormant would lose their tolerance for the antimicrobial agent as substrate becomes available. Using a three-dimensional computer model of biofilm dynamics, this study investigates the level of protection that could be explained by substrate limitation when a biofilm is exposed to a growth-dependent antimicrobial agent.

Materials and Methods

The computer model, BacLAB, used in this study has been described in detail elsewhere (7). This model uses a hybrid modeling approach in which all soluble components are modeled using discretized differential equations and the individual microorganisms that compose the biofilm are modeled discretely using a cellular automata algorithm. The advantage to the hybrid approach is the ability to separate different biofilm processes according to their natural time scale and that the aggregate behavior of the biofilm is emergent from the local interactions between individual microorganisms. Some of the processes simulated by the computer model include diffusion of soluble components into the biofilm, substrate consumption, microbial growth, and biofilm detachment resulting from substrate starvation. Parameter values are summarized in Table 4-1.

Table 4-1. Kinetic and diffusion parameters used in the simulations.

Parameter	Symbol	Value	Unit(s)
Maximum specific growth rate	μ_{max}	0.3	h^{-1}
Time step	Δt	1.0	h
Bulk substrate concentration	$C_{S,bulk}$	8.0	$g\ m^{-3}$
Diffusivity of the antimicrobial in the aqueous phase (including the liquid, channels and voids)	$D_{A,aq}$	$1.51 \cdot 10^{-6}$	$m^2\ h^{-1}$
Relative effective diffusivity of the antimicrobial in biofilm	$D_{A,e} / D_{A,aq}$	0.2	
Diffusivity of substrate in the aqueous phase (including the liquid, channels and voids)	$D_{S,aq}$	$7.20 \cdot 10^{-6}$	$m^2\ h^{-1}$
Relative effective diffusivity of substrate in biofilm	$D_{S,e} / D_{S,aq}$	0.55	
Local nutrient concentration threshold	$C_{S,min}$	1.0	$g\ m^{-3}$
Monod half saturation coefficient	K_S	0.1	$g\ m^{-3}$
Average cell mass	m_{avg}	$1.75 \cdot 10^{-13}$	g
Number of initial colonies	N_c	28	
Number of nodes in x-direction	N_x	300	
Number of nodes in y-direction	N_y	300	
Radius of initial colonies	R_c	8.55	μm
Limiting substrate	S	Oxygen	
Duration of time below $C_{S,min}$ before detachment	t_{detach}	24	h
Yield coefficient	Y_{XS}	0.24	$g_X\ g_S^{-1}$

Antimicrobial Penetration

The time course of penetration of the antimicrobial agent into the biofilm was calculated in two ways. A lower bound was calculated by neglecting external mass transfer (i.e. C_A/C_{A0}=1 everywhere outside the biofilm) and solving for the transient diffusion into the biofilm using a finite difference solution to

$$\frac{\partial C_A}{\partial t} = D_{A,e} \cdot \nabla^2 C_A \qquad (4\text{-}1)$$

$$C_A = 0 \text{ inside biofilm for } t \le 0 \tag{4-2}$$

$$C_A = C_{A0} \text{ outside biofilm for all } t \tag{4-3}$$

$$\text{at } z = 0, \frac{\partial C_A}{\partial z} = 0 \text{ for all } t > 0 \tag{4-4}$$

$$\text{periodic boundaries on } x \text{ and } y \text{ for all } z \ge 0 \text{ and } t > 0 \tag{4-5}$$

where C_A is the concentration of the antimicrobial, C_{A0} is the concentration of antimicrobial in the bulk fluid, t is time, and $D_{A,\mathrm{e}}$ is the effective diffusion coefficient of the antimicrobial in the biofilm.

A more conservative estimate of the antimicrobial penetration, the upper bound, can be generated solving Equation (4-1) with a boundary layer of 50 μm which provides external mass transfer resistance subject to the following initial and boundary conditions:

$$C_A = 0 \text{ for all } x, y, z \text{ and } t \le 0 \tag{4-6}$$

$$\text{at } z = z_{\max}, C_A = C_{A0} \text{ for all } x, y \text{ and } t > 0 \tag{4-7}$$

$$\text{at } z = 0, \frac{\partial C_A}{\partial z} = 0 \text{ for all } t > 0 \tag{4-8}$$

$$\text{periodic boundaries on } x \text{ and } y \text{ for all } z \ge 0 \text{ and } t > 0 \tag{4-9}$$

By using the effective diffusion coefficient in the biofilm, $D_{A,\mathrm{e}}$, both inside and outside the biofilm, Equation (4-1) reduces to one-dimension with all gradients in the z-direction. While diffusion is certainly faster in the bulk fluid, this conservative estimate allows the argument that the true solution is safely between the aforementioned upper and lower bounds.

Antimicrobial Tolerance

The time scale associated with microbial processes (e.g., cellular division, death, movement, etc.) is on the order of a few hours. In this investigation, we assumed that the biofilm is rapidly and completely penetrated by the antimicrobial agent. The justification for this assumption is the calculation of diffusive penetration of the antimicrobial agent outlined above and is formally presented in the Results and Discussion section. Killing by the antimicrobial agent in the biofilm was calculated using a probability of death in the presence of the antimicrobial presence for a single time step of 1 h. At each time step that the antimicrobial agent is present, every cell in the simulation generates a random number from a uniform distribution on the interval [0, 1]. If the random number is less than or equal to the probability of killing, the cell dies and remains metabolically inactive for the remainder of the simulation or until it detaches from the biofilm. Otherwise, the cell continues to function normally.

Two base case simulation studies were conducted without any antimicrobial resistance mechanisms. In these studies, each cell in the simulation has the same probability of death when exposed to an antimicrobial agent. Therefore, inclusion within a biofilm provides no additional protection over suspended cells in culture. Both studies included ten replicate simulations of 500 h in which the presence the antimicrobial agent was simulated for 12 continuous hours. They differed only in the point of biofilm development at which the antimicrobial was introduced. The first study introduced the antimicrobial at 100 h of biofilm development corresponding to the end of the log growth phase. The second study introduced the agent after the simulated biofilm had reached a pseudo steady-state at 200 h. For both studies the probability of killing due to the

presence of the antimicrobial agent was 0.6838 for a 1 h interval. This value was calculated so as to provide a 6 log reduction in non-growing suspended cell cultures in a 12 h treatment period by solving the following equality

$$Log_{10}[X_0] - Log_{10}[X_0 \cdot (1-P)^{12}] = 6 \tag{4-10}$$

where P is the probability of killing, and X_0 is the number of viable cells at the beginning of treatment.

To probe the degree of protection that could be expected from a substrate-dependent antimicrobial agent, the aforementioned simulation studies were repeated with one modification. The antimicrobial efficacy was simulated to be proportional to the amount of substrate available to the microorganism. That is,

$$P = \frac{P_{MAX}}{C_{S0}} \cdot C_S \tag{4-11}$$

where P_{MAX} is the maximum probability of killing and equal to the probability of killing used in the base case simulations, C_{S0} is the substrate concentration in the bulk fluid, and C_S is the local substrate concentration at a particular cell. Thus cells in substrate rich regions of the biofilm have the lowest antimicrobial tolerance, whereas cells in substrate depleted regions are expected to be tolerant to antimicrobial killing.

Finally, to identify the treatment period necessary to eradicate a biofilm with a growth dependent antimicrobial agent, the simulation studies relating the antimicrobial efficacy to the local substrate concentration were duplicated with antimicrobial treatment continuing beyond the 12 h treatment period used in the previous studies. This time the presence of the antimicrobial continued until viable cells were eliminated from the biofilm.

Results and Discussion

Antimicrobial Penetration

An antimicrobial agent with an effective diffusion coefficient of 8.4×10^{-7} cm^2 s^{-1} was calculated to penetrate throughout the mature biofilm within a few minutes (Figure 1). The calculation assumed that there was no reactive neutralization of the antimicrobial agent. We sought to place bounds on the penetration time. The most rapid penetration was calculated by neglecting external mass transfer resistance. In other words, the bulk fluid concentration of antimicrobial was imposed on all surfaces of the biofilm. In this case, the time for the antimicrobial agent to permeate throughout the biofilm to a concentration of 90 percent or greater of the applied bulk fluid concentration was 14.8 seconds (Figures 4-1 and 4-2). To determine an upper bound on the antimicrobial penetration time, external mass transfer resistance was included and the same value of the diffusion coefficient used inside the biofilm was used outside the biofilm. The time required for the antimicrobial agent to attain 90 percent or greater of the dosed concentration everywhere in the biofilm was 158.9 s in this calculation. These calculations show that penetration of a non-reacting antimicrobial occurs quickly relative to the processes of growth, killing, and detachment. As such, the transient diffusion of the antimicrobial agent into the biofilm need not be modeled. This conclusion is in agreement with previous analyses (13). In subsequent simulations, the bulk fluid concentration was applied everywhere within the biofilm at the onset of the antimicrobial dosing period and maintained for the duration of the dose.

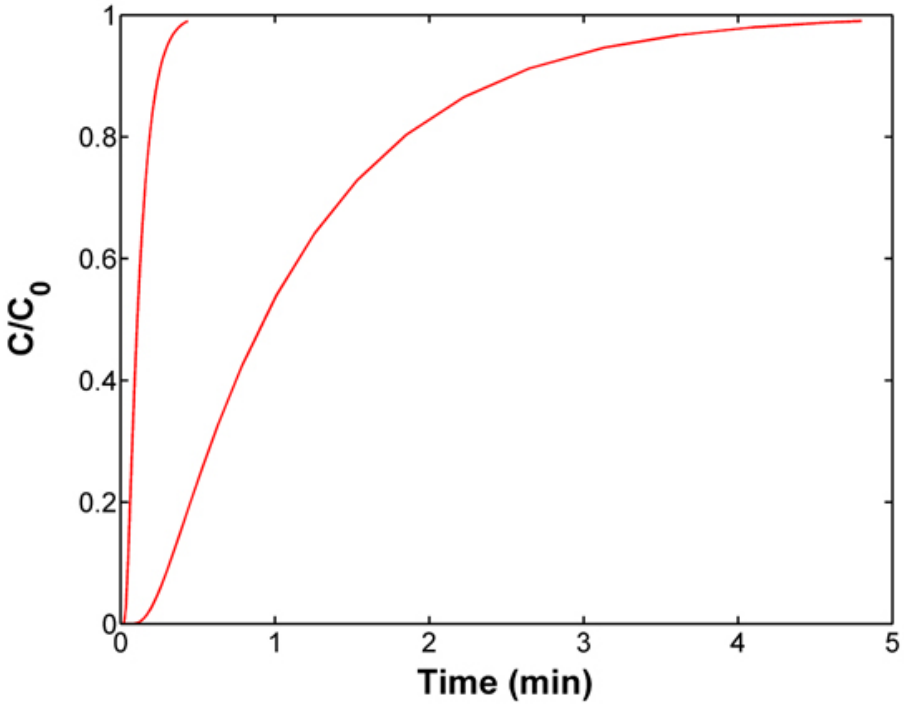

Figure 4-1. Transient penetration of a non-reacting antimicrobial agent into biofilm. The minimum concentration within the biofilm is represented as C_{min}/C_o versus time. The leftmost curve represents the minimum concentration when neglecting external mass transfer and the rightmost curve represents the concentration when a 50 μm boundary layer is present.

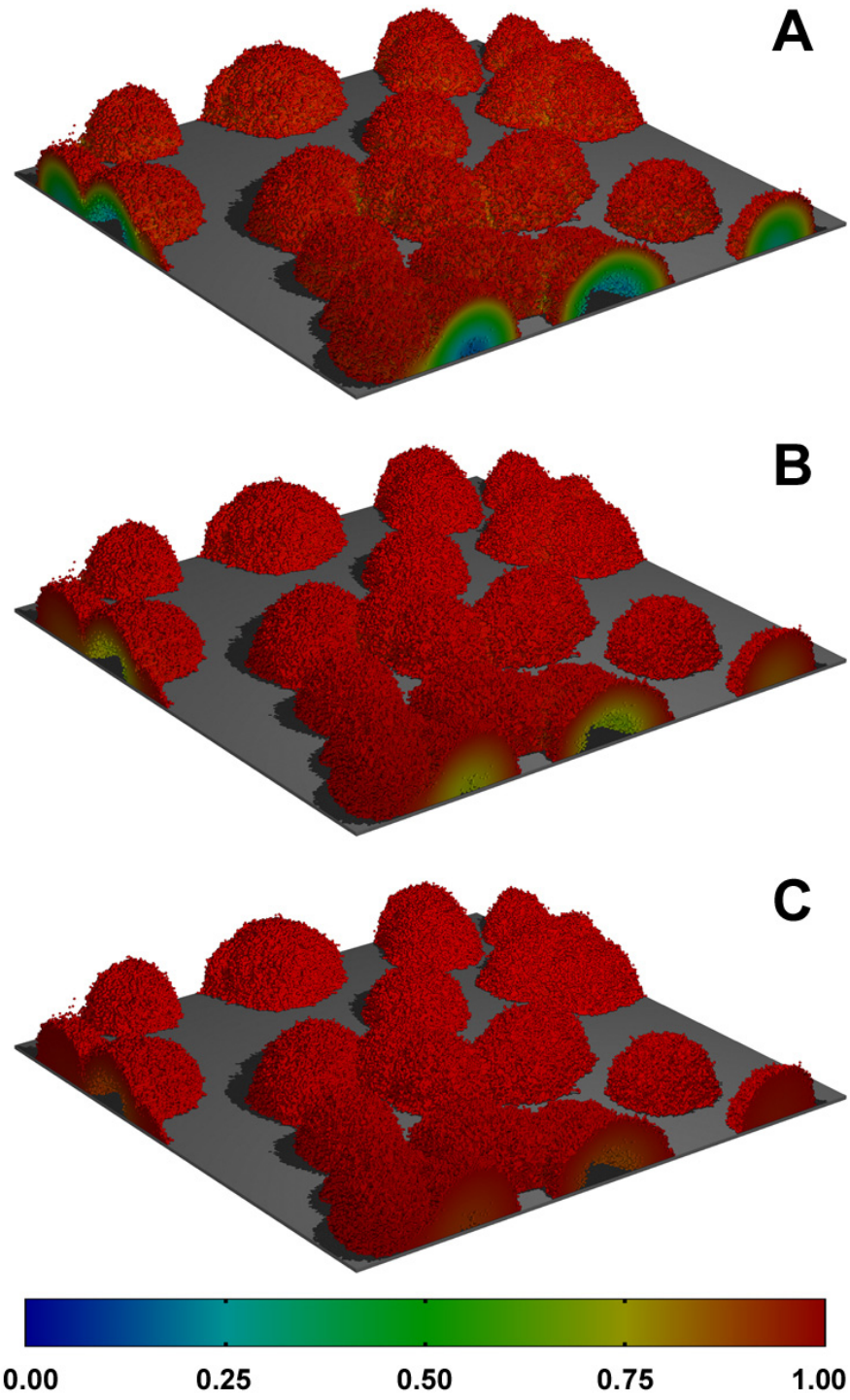

Figure 4-2. Penetration of antimicrobial agent into a biofilm with an areal cell density of 3.25×10^8 cells cm^{-2} and a maximum thickness of 64 μm. The antimicrobial concentration is represented as C/C_o and penetration is shown at 2.5, 7.5, and 12.5 seconds (A-C) following the introduction of antimicrobial agent. This simulation neglects external mass transfer resistance as explained in the text.

Antimicrobial Tolerance

The computer model used in this investigation simulated biofilm development, and the response to antimicrobial treatment, over a period of 500 h. Some of the features captured in these simulations included dynamic development of three-dimensional, heterogeneous biofilm structures, gradients in substrate concentration leading to regions of substrate depletion in the interior of large cell clusters, variable killing by antimicrobial agent from one simulation to the next, greater killing of cells at the periphery of cell clusters compared to those cells which were more deeply embedded, and reduced overall antimicrobial susceptibility of cells in the biofilm. A representative video of one simulation can be viewed at http://www.erc.montana.edu/Res-Lib99-SW/pubs/Theses/Database/TD_DisplayScript.asp.

We selected a value for the antimicrobial kill rate that corresponded to a 6 log reduction in viable cell numbers after 12 h exposure of planktonic cells to the antimicrobial agent in the absence of cell growth. Assuming that surviving cells continue to grow during antimicrobial exposure, the net log reduction predicted for planktonic cells will be 4.44. We anticipated a similar degree of killing would be predicted by the biofilm model when killing was made independent of the local substrate concentration. This proved to be the case, with the simulations predicting near complete killing of the biofilm. When the antimicrobial treatment began at 100 h, the simulated biofilms had an average live cell areal density of 3.1×10^8 cells/cm^2 (s.e. = 9.1×10^6) which was reduced to 531 cells/cm^2 following 12 h of treatment. Similarly when the treatment began at 200 h, the simulated biofilms averaged 8.6×10^7 live cells/cm^2 (s.e. = 3.4×10^7) with these numbers falling to 114 cells/cm^2. The average log reductions were 6.26 ± 1.18 and 7.13

± 1.83 for the 100 h and 200 h old biofilms respectively. These values are slightly larger than the planktonic log reduction of 4.44 because the average growth of biofilm cells is less than the growth rate of planktonic cells and also because detachment of biofilm cells enhances the log reduction. These simulations demonstrate that when the rate of antimicrobial killing is assumed to be independent of the substrate concentration inclusion within a biofilm provides no additional protection.

When antimicrobial efficacy was assumed to be proportional to the local substrate concentration, the predicted time course of biofilm killing and recovery was as shown in Figure 3. When the 12 h antimicrobial dose was administered at both 100 h (Figure 4-3A) and 200h (Figure 4-3B) of biofilm development, dead cell numbers rapidly increased within the biofilm. At the end of the antimicrobial dose period, the dead cell numbers remained constant for a period of approximately 37 to 117 h. During this time, surviving cells grew and little detachment occurred. Detachment events eventually began to remove dead cells from the biofilm, a process that took 200 to 300 h to complete. The extent of killing, expressed as a log reduction, was approximately 0.5 when antimicrobial treatment was initiated at 100 h (Figure 4-3C) and ranged from 0.45 to 1.6 when treatment began at 200 h (Figure 4-3D). These log reductions are considerably less than those calculated for free-floating cells exposed to the bulk fluid concentration of substrate. Somewhat more killing was recorded for the 200 h old biofilms on average than for the 100 h old biofilms. The modest difference in susceptibility can most likely be attributed to larger and/or more frequent detachment events occurring during treatment of the 200 h old biofilm.

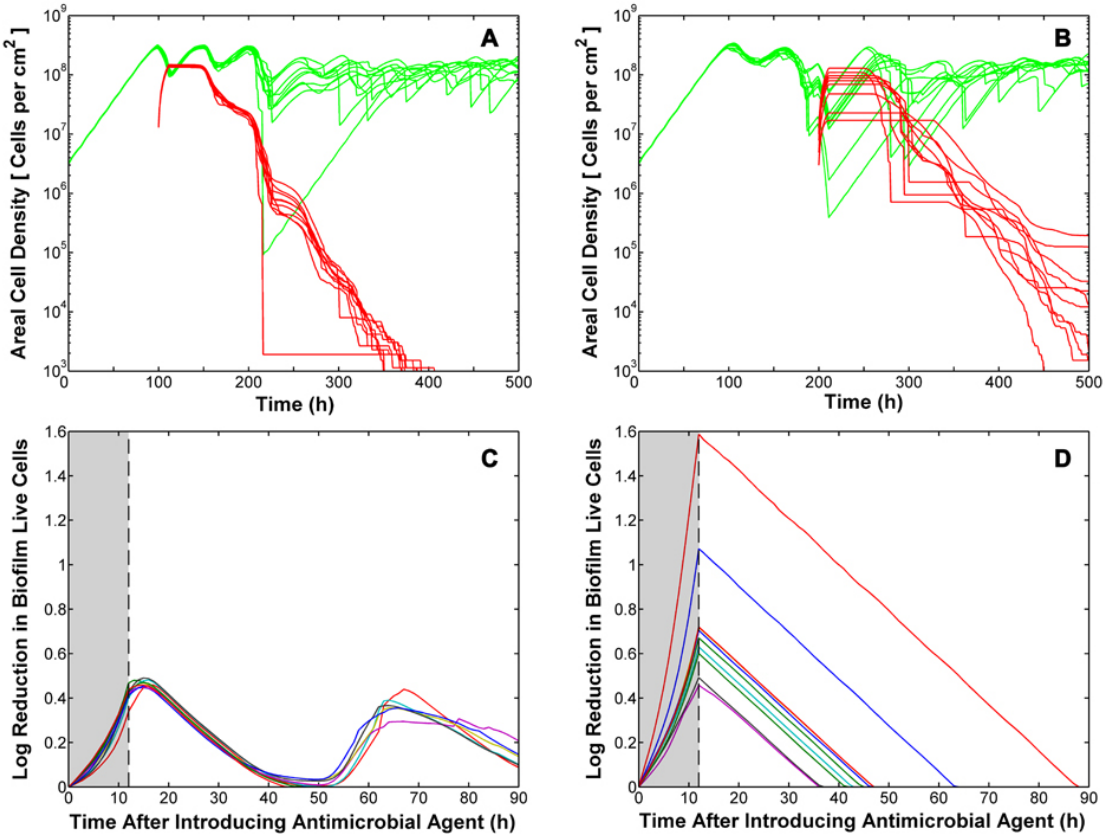

Figure 4-3. Simulated killing and recovery of cells in a biofilm exposed to an antimicrobial agent expressed in terms of areal cell density (A and B) and log reduction (C and D). Green lines denote total cell numbers and red lines denote dead cell numbers. The antimicrobial treatment was applied for 12 h (shading) after either 100 h (A and C) or 200 h (B and D) of biofilm development. Ten replicate simulations are plotted.

These results are consistent with the idea that microorganisms within a biofilm are afforded some degree of protection from antimicrobial agents whose action is dependent on the availability of a metabolic substrate. Predicted substrate concentrations in representative cross sections are shown in Figure 4-4. These gradients confirm that lower substrate concentrations prevail closer to the substratum and in the vicinity of cell clusters.

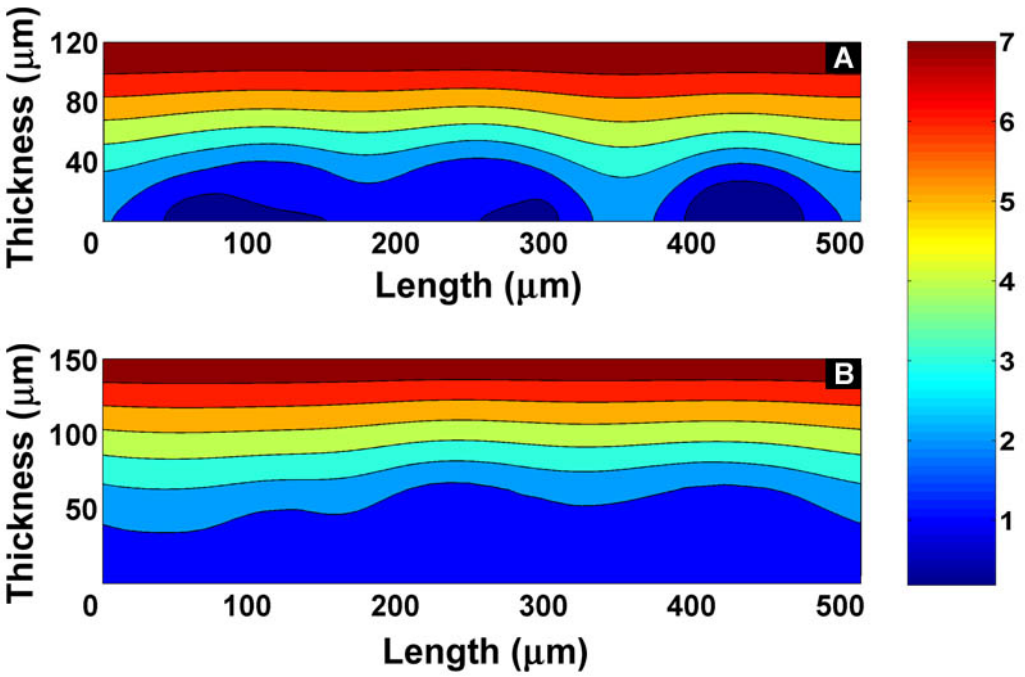

Figure 4-4. Substrate concentration in representative biofilm cross sections after 100 h (A) or 200 h (B) of biofilm development. These substrate profiles correspond to the biofilm structures shown in Figures 4-5A and 4-5B, respectively.

Consistent spatial patterns of killing within the denser biofilms, those that were 100 h old at the onset of treatment, were noted (Figures 4-5A-C). There was an apparent higher rate of killing near the surface when compared to the cell cluster interiors. This is explained by the higher substrate concentration at the cluster-bulk fluid interface and the depletion of substrate in the cell cluster interiors (Figure 4-4). In the 200 h old biofilms, no spatial organization of killing patterns could be discerned when examining cross sections (Figures 4-5D-F). These biofilms were characterized by significant voids and loosely tethered clusters in which the substrate concentration was more uniformly distributed (Figure 4-4).

Plotting the fraction of dead cells as a function of distance from the substratum (Figure 4-6A) illustrates that the spatial trends observed in the 100 h biofilm (Figures 4-5A-C) are consistent throughout the replicate simulations. However, Figure 4-6B

suggests a weak spatial pattern to killing within the biofilm not observed in the in Figures 4-5D-F. One possible factor contributing to the weak correlation when compared to the 100 h biofilm is more frequent detachment events occurring in nutrient deficient regions that result in sloughing of these loosely tethered clusters during antimicrobial treatment. These are the same regions of the biofilm that would better tolerate antimicrobial treatment. The detachment leads to better penetration of the substrate, which contributes to antimicrobial efficacy.

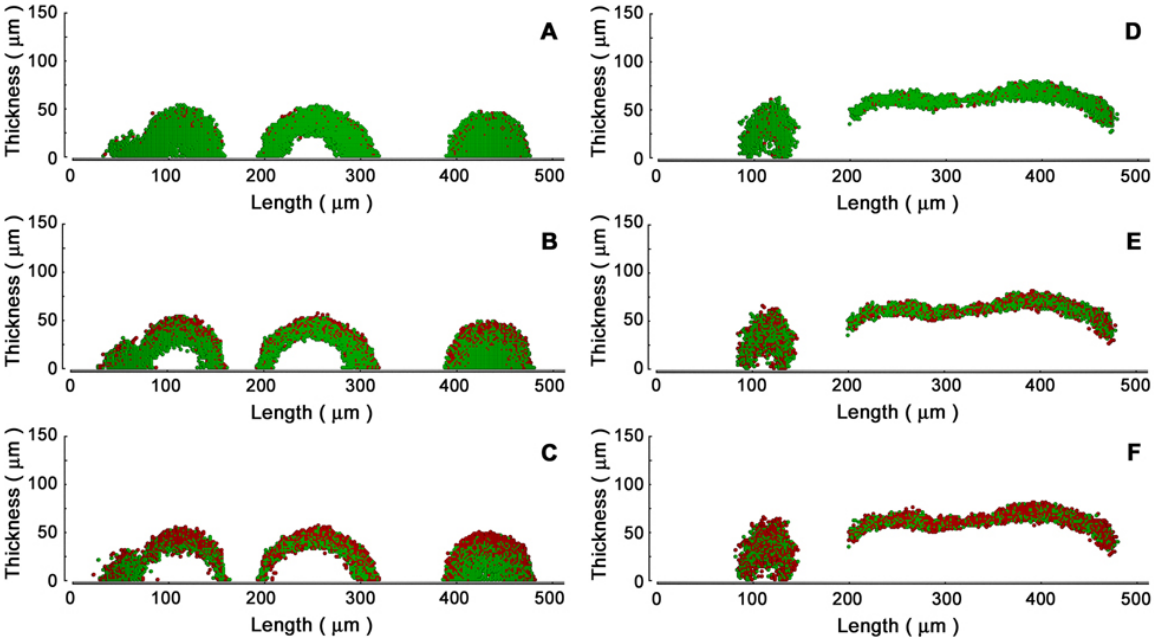

Figure 4-5. Live (green) and dead (red) cell distributions in biofilm cross sections at 1, 6, and 11 h after introduction of the antimicrobial agent. Figures A-C and D-F are representative of simulations when treatment begins at 100 h and 200 h, respectively.

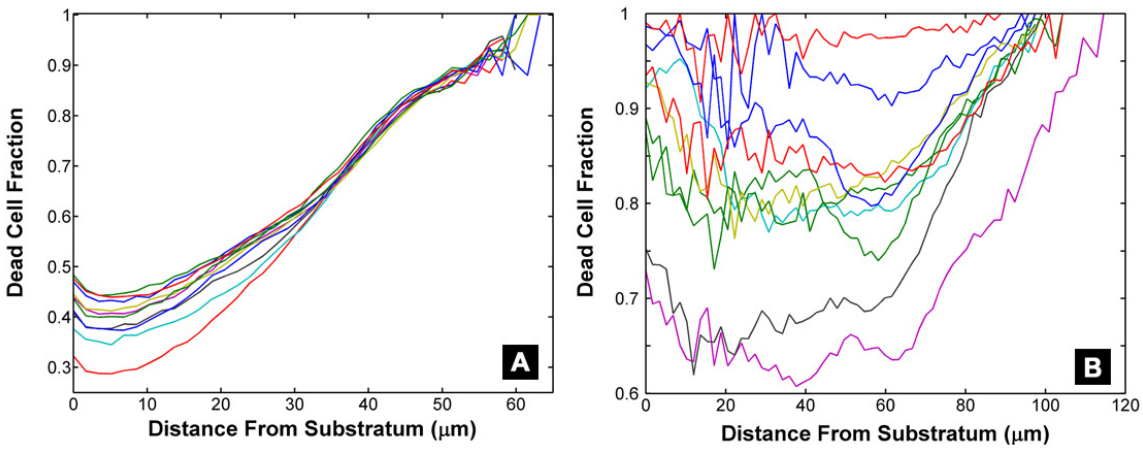

Figure 4-6. Dead cell fractions as a function of distance from the substratum following treatment beginning at 100 h (A) and 200 h (B). Ten replicate simulations are plotted.

One of the interesting features of this computer model is that it does not return the same answer every time. Opportunities for variation between runs include the initial pattern in which the substratum is seeded with microorganisms, displacement of neighboring cells when a new cell is created, and antimicrobial killing. Each of these constituent phenomena has a stochastic element associated with it. The random behaviors lead to different biofilm structures each time the model is run, and different distributions of live and dead cells within these structures. The variation that is predicted by this model is reminiscent of that described by experimenters. For example, the mean log reduction and standard deviation of this reduction for 200 h old biofilms subjected to 12 h antimicrobial treatment was 0.77 ± 0.33. This standard deviation is similar to that reported for biofilm disinfection studies (22).

In simulations where antimicrobial treatment continued until biofilm extinction, complete killing of the biofilm took 43.4 ± 2.2 h and 43.9 ± 5.9 h when treatment began at 100 h and 200 h respectively. In other words, the model predicts that the biofilm does eventually succumb to the antimicrobial treatment (Figure 4-7). Since many real biofilms

survive even prolonged antimicrobial exposure, substrate-limited killing may not be a sufficient explanation for the antimicrobial tolerance of biofilms in engineered systems and medical settings. Simulations suggest that substrate limitation has the potential to retard antimicrobial killing but cannot explain sustained tolerance. One of the features predicted by the model is that killing should accelerate at some point during the treatment (Figure 4-7B). This behavior is rarely observed experimentally. We therefore suggest that substrate limitation in biofilms is a plausible contributing factor to the reduced antimicrobial susceptibility in biofilms, but is probably not adequate by itself to account for the full degree of protection afforded to microorganisms in biofilms.

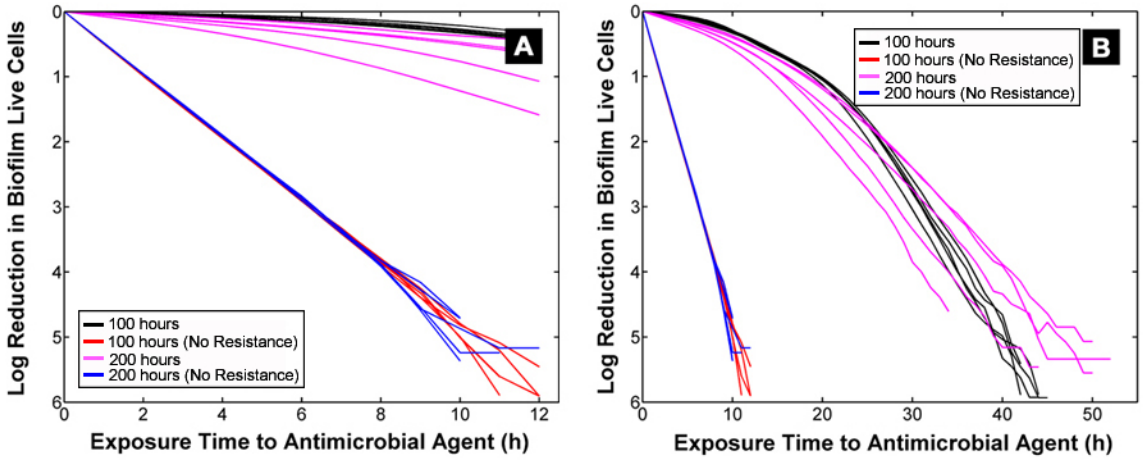

Figure 4-7. Biofilm killing by continuous antimicrobial exposure over 12 h (A) or until eradication of the biofilm (B). Dead cell fraction as a function of distance from the substratum when treatment begins at 100 h and 200 h. Five replicate simulations are plotted.

References

1. **Anderl, J. N., M. J. Franklin, and P. S. Stewart.** 2000. Role of antibiotic penetration limitation in *Klebsiella pneumoniae* biofilm resistance to ampicillin and ciprofloxacin. Antimicrob. Agents Chemother. **44:**1818-1824.

2. **Brown, M. R., D. G. Allison, and P. Gilbert.** 1988. Resistance of bacterial biofilms to antibiotics: a growth-rate related effect? J Antimicrob Chemother **22:**777-80.

3. **Darouiche, R. O., A. Dhir, A. J. Miller, G. C. Landon, I. I. Raad, and D. M. Musher.** 1994. Vancomycin penetration into biofilm covering infected prostheses and effect on bacteria. J Infect Dis **170:**720-723.

4. **Davies, D.** 2003. Understanding biofilm resistance to antibacterial agents. Nature Reviews Drug Discovery **2:**114-122.

5. **de Beer, D., P. Stoodley, F. Roe, and Z. Lewandowski.** 1994. Effects of biofilm structures on oxygen distribution and mass-transport. Biotechnol. Bioeng. **43:**1131-1138.

6. **Dunne, W. M., E. O. Mason, and S. L. Kaplan.** 1993. Diffusion of rifampin and vancomycin through a *Staphylococcus-epidermidis* biofilm. Antimicrob. Agents Chemother. **37:**2522-2526.

7. **Hunt, S. M., M. A. Hamilton, J. T. Sears, G. Harkin, and J. Reno.** 2003. A computer investigation of chemically mediated detachment in bacterial biofilms. Microbiol. **149:**1155-63.

8. **Lewis, K.** 2001. Riddle of biofilm resistance. Antimicrob. Agents Chemother. **45:**999-1007.

9. **Mah, T. C., and G. A. O'Toole.** 2001. Mechanisms of biofilm resistance to antimicrobial agents. Trends Microbiol. **9:**34-39.

10. **Roberts, M. E., and P. S. Stewart.** 2004. Modeling antibiotic tolerance in biofilms by accounting for nutrient limitation. Antimicrob. Agents Chemother. **48:**48-52.

11. **Shigeta, M., G. Tanaka, H. Komatsuzawa, M. Sugai, H. Suginaka, and T. Usui.** 1997. Permeation of antimicrobial agents through *Pseudomonas aeruginosa* biofilms: A simple method. Chemotherapy **43:**340-345.

12. **Sternberg, C., B. B. Christensen, T. Johansen, A. Toftgaard Nielsen, J. B. Andersen, M. Givskov, and S. Molin.** 1999. Distribution of bacterial growth activity in flow-chamber biofilms. Appl Environ Microbiol **65:**4108-17.

13. **Stewart, P.** 1996. Theoretical aspects of antibiotic diffusion into microbial biofilms. Antimicrob. Agents Chemother. **40:**2517-2522.

14. **Stewart, P. S.** 1994. Biofilm accumulation model that predicts antibiotic resistance of *Pseudomonas aeruginosa* biofilms. Antimicrob. Agents Chemother. **38:**1052-1058.

15. **Stewart, P. S.** 2002. Mechanisms of antibiotic resistance in bacterial biofilms. Int. J. Med. Microbiol. **292:**107-113.

16. **Stewart, P. S., and J. W. Costerton.** 2001. Antibiotic resistance of bacteria in biofilms. Lancet **358:**135-138.

17. **Stewart, P. S., M. A. Hamilton, B. R. Goldstein, and B. T. Schneider.** 1996. Modeling biocide action against biofilms. Biotechnol. Bioeng. **49:**445-455.

18. **Stewart, P. S., J. Rayner, F. Roe, and W. M. Rees.** 2001. Biofilm penetration and disinfection efficacy of alkaline hypochlorite and chlorosulfamates. J. Appl. Microbiol. **91:**525-32.

19. **Suci, P. A., M. W. Mittelman, F. P. Yu, and G. G. Geesey.** 1994. Investigation of ciprofloxacin penetration into *Pseudomonas-aeruginosa* biofilms. Antimicrob. Agents Chemother. **38:**2125-2133.

20. **Wentland, E. J., P. S. Stewart, C. T. Huang, and G. A. McFeters.** 1996. Spatial variations in growth rate within *Klebsiella pneumoniae* colonies and biofilm. Biotechnol. Progr. **12:**316-321.

21. **Xu, K. D., P. S. Stewart, F. Xia, C. T. Huang, and G. A. McFeters.** 1998. Spatial physiological heterogeneity in *Pseudomonas aeruginosa* biofilm is determined by oxygen availability. Appl Environ Microbiol **64:**4035-9.

22. **Zelver, N., M. Hamilton, D. Goeres, and J. Heersink.** 2001. Development of a standardized antibiofilm test. Methods Enzymol **337:**363-76.

23. **Zheng, Z. L., and P. S. Stewart.** 2002. Penetration of rifampin through *Staphylococcus epidermidis* biofilms. Antimicrob. Agents Chemother. **46:**900-903.

CHAPTER 5

CONCLUSIONS

This dissertation presented a modeling approach suitable for exploring conjectures at the microbial level. The model was used to investigate three conjectures pertaining to biofilm detachment and recalcitrance to antimicrobial agents. The four research objectives listed in Chapter 1 were addressed in three separate but interrelated manuscripts that compose the main body of this dissertation. This chapter briefly summarizes those results, discusses the broader issue of the contributions this type of model brings to biofilm research, and provides suggestions for the further development of the model.

Summary of Results

Chapters 2 and 3 investigated two potential triggers for biofilm detachment: accumulation of a metabolic product and the depletion of a metabolic substrate. When implemented into the model, both mechanisms predicted similar biofilm behavior and structures that agree qualitatively with experimental observations. In retrospect, the similarities between these two mechanisms are somewhat intuitive and are explained as follows. Regions in the biofilm where diffusive egress of a soluble microbial product is most restricted correspond to the same regions in the biofilm that are nutrient deficient. Thus, accumulation of a metabolic product (i.e., signaling molecule) will occur in the same regions of a biofilm that are devoid of nutrients. Some of the phenomena predicted

in these simulation studies included gradients in substrate concentration and growth rate, hollow cell clusters, and biofilm sloughing. Furthermore, the simulated biofilms were able to reach an oscillatory steady-state where the biofilms were maintained as heterogeneous entities by constant growth and periodic detachment.

In Chapter 4, the model was adapted to simulate the protection from killing by antimicrobial agents afforded to microorganisms in the biofilm state. Because antimicrobials are thought be more effective in killing actively growing bacteria, the rate of killing was assumed to be proportional to the local concentration of the substrate. Results predicted that when exposed to an antimicrobial for 12 hours, a biofilm would experience log reductions ranging from 0.34 to 1.59, whereas free-floating cells in the bulk fluid would experience nearly a 4.44 log reduction for the same treatment. The model also predicted that a biofilm relying on only substrate limitation for protection would eventually succumb to antimicrobial treatment, only at a much slower rate than its free-floating counterparts. These results suggest that substrate limitation has the potential to contribute to the reduced antimicrobial susceptibility found in biofilms, but is not adequate by itself in explaining the log-term persistence of biofilm viability observed experimentally.

Contribution to Biofilm Research

Mathematical models are valuable tools in the investigation of biofilm phenomena. There are numerous models currently being used in biofilm research but most either attempt to fully define specific biofilm systems or focus on completely

describing a single phenomenon associated with biofilm development. As stated in Chapter 1, an objective for this research was to develop a base model that is well suited to investigate a variety of conjectures about how specific processes at the biological level affect biofilm structure and/or function. Furthermore, the model structure should be such that it facilitates communication across discipline boundaries and serves to complement experimental investigation. The model presented in this dissertation achieves these objectives.

This model provides several firsts in biofilm modeling. It is the only biofilm model to consider biological mechanisms of detachment and the potential environmental cues that trigger them. It predicts hollow clusters and structural heterogeneity ensuing from negative processes, like detachment. It provides potential biological explanations contributing to biofilm sloughing. And finally, it is the first three-dimensional investigation of antimicrobial action against biofilms.

The computer model is founded on well-established transport equations but structured to provide the plasticity needed for practical use as a research tool. This plasticity arises from the use of cellular automata to describe how microorganisms within the biofilm interact with one another and in response to their local environment. The use of cellular automata also facilitates communication with other scientists by allowing insight to be provided without requiring traditional mathematics. The simulation studies conducted in Chapters 2-4 demonstrate that the model can predict many of the same phenomena observed experimentally, and that the model can be adapted to test a variety of postulated biofilm mechanisms. Subsequent work by other researchers has already

begun to adapt the model to investigate the fate of pathogens in a drinking water biofilm and the theory of a "persister" cell phenotype to explain biofilm tolerance to antimicrobial agents.

There may be several mechanisms that contribute to an observed phenomenon, but the mechanisms are often difficult or impossible to separate experimentally. Theoretical studies allow researchers to investigate the expected contribution of an individual mechanism to an observed function or phenotype.

Another not so obvious contribution of this modeling work is the ability to visualize and communicate the effects of individual processes on a biofilm. The ability to take a "snap shot" of a simulated biofilm and visually demonstrate the results of these investigations is a powerful communication tool.

Future Work

The strength of this model lies in its relative simplicity. It does not attempt to include all conventional biofilm processes for the sake of completeness. However, this does not imply that other processes not included in the model do not contribute significantly to biofilm dynamics, only that they were not required for the conjectures considered in this dissertation. That said, improvements to the existing model can be made in two ways: adding additional processes to the model and improving the implementation of the existing processes.

Potential Processes for Inclusion into the Model

- Hydrodynamics – Hydrodynamics have a significant impact on biofilm structure and detachment. High liquid velocities imply high shear forces at the biofilm surface that could conceivably lead to increased detachment and thinner more homogeneous structures. However, accounting for fluid flow in three-dimensions around irregular structures is a complicated problem and little is still known about the mechanical properties of biofilms. The inclusion of fluid flow into a model of this sort would be a significant contribution but should only be considered if the expected results warrant the increase in model complexity and computational resources.

- Surface Erosion – The erosion of microorganisms from the surface of biofilms is well established. However, the model in its current state has no mechanism for detachment from the surface of the biofilm. The simple process of identifying the number of "neighbors" a microorganism has could determine if a microorganism is at the surface. At that point a small finite probability of detaching from an appropriate distribution applied to those on the surface could serve as a rule for surface erosion.

- Attachment/Adsorption – The only process considered in this modal to contribute to biofilm accumulation is microbial growth. It is intuitive that when microorganisms detach from a biofilm, at some point they either adsorb to a clean surface or reattach to a biofilm elsewhere. While this is not commonly observed in laboratory systems the adsorption and attachment of microorganisms is generally accepted to contribute to microbial accumulation. As such, the process of attachment/adsorption could be

included by making the rate of attachment/adsorption proportional to the concentration of cells in the bulk fluid.

Improvements to the Implementation of Existing Processes

- Search for Hanging Clusters – As this work was concluding, I uncovered a deficiency in the algorithm used to identify hanging clusters. In some instances, the algorithm was not able to trace some cells in loosely tethered clusters back to the substratum and incorrectly detached them from the biofilm. The effect appears to be minor, and the qualitative results presented in this dissertation are valid. Due to the stochastic nature of these simulations, the precise quantitative effect on the simulation studies is impossible to determine. The algorithm has been fixed.

- Solver – The current solver used to solve Equation 2.1 for the diffusive transport within the biofilm is a subroutine from the FISHPACK library written in Fortran. Implementation of the solver within the code is a non-trivial issue and the inclusion of an external Fortran library is antagonistic to the object-oriented programming style of C++. A solver written in C++ would adhere to the object-oriented style of the existing code and allow future developers the opportunity to make simple modifications to the source (e.g., checking for negative concentration values) without the overhead of learning to program in Fortran.

- Computational Grids – Currently there is a one-to-one correspondence between lattice points on which solute concentrations are calculated and cubes containing the microorganisms as described in Chapter 2. By reducing the number of lattice points

by a factor of 2 or more on which solute concentrations are calculated and interpolating to find solute concentrations at cubes between points, simulation speed could be drastically improved.

- User Defined Functions – As this model is used to investigate different conjectures associated with biofilms it will inevitably be modified by a variety of researchers. One strategy to keep the fundamental structure of the model intact and thus its flexibility would be to incorporate a procedure that allows users the option to define functions at runtime pertaining to different biofilm processes (e.g., kinetic functions, detachment rules, movement rules, etc.). This would ultimately require the development of some type of interface (not necessarily graphic) that allows users to write functions and dynamically link them with the model.

APPENDICES

APPENDIX A

SOLUTION TO THE REACTION DIFFUSION EQUATION

The solution to the three-dimensional reaction diffusion equation using the POIS3D subroutine was non-trivial and warrants additional discussion. Some of the factors that contributed to the difficulty were: a discontinuity in the diffusion coefficients between the bulk fluid and biomass, the irregular structure of the biofilm and the need to apply a reaction term to nodes containing biomass, and the nonlinearity of the reaction term. The solution method used in the preceding chapters is presented below.

Numerical Solution to the Reaction Diffusion Equation

Equation (A-1) is the three-dimensional representation for the transient diffusive transport and reaction of a solute. Let C_i denote the concentration of solute i, t denote time, D_i denote the diffusivity coefficient of solute i, and r_i denote the reaction rate of solute i.

$$\frac{\partial C_i}{\partial t} = D_i\left(\frac{\partial^2 C_i}{\partial x^2} + \frac{\partial^2 C_i}{\partial y^2} + \frac{\partial^2 C_i}{\partial z^2}\right) + r_i \tag{A-1}$$

A Crank-Nicoloson scheme that is second order accurate in both time and space was used to solve Equation (A-1) in this dissertation. This approach approximates the temporal derivative at $t^{n+1/2}$ as

$$\frac{\partial C_i}{\partial t} \cong \frac{C_i^{n+1}(x,y,z) - C_i^{n}(x,y,z)}{\Delta t} \tag{A-2}$$

where n is the current time step (or iteration). The second derivative in space is then approximated at the midpoint by averaging the central difference approximations at t^n and t^{n+1}as shown in Equations (A-3)-(A-5).

$$\frac{\partial^2 C_i}{\partial x^2} \cong \frac{1}{2}\left(\frac{C_i^n(x+1,y,z) - 2C_i^n(x,y,z) + C_i^n(x-1,y,z)}{\Delta x^2} + \cdots \right.$$
$$\left. \frac{C_i^{n+1}(x+1,y,z) - 2C_i^{n+1}(x,y,z) + C_i^{n+1}(x-1,y,z)}{\Delta x^2} \right) \tag{A-3}$$

$$\frac{\partial^2 C_i}{\partial y^2} \cong \frac{1}{2}\left(\frac{C_i^n(x,y+1,z) - 2C_i^n(x,y,z) + C_i^n(x,y-1,z)}{\Delta y^2} + \cdots \right.$$
$$\left. \frac{C_i^{n+1}(x,y+1,z) - 2C_i^{n+1}(x,y,z) + C_i^{n+1}(x,y-1,z)}{\Delta y^2} \right) \tag{A-4}$$

$$\frac{\partial^2 C_i}{\partial z^2} \cong \frac{1}{2}\left(\frac{C_i^n(x,y,z+1) - 2C_i^n(x,y,z) + C_i^n(x,y,z-1)}{\Delta z^2} + \cdots \right.$$
$$\left. \frac{C_i^{n+1}(x,y,z+1) - 2C_i^{n+1}(x,y,z) + C_i^{n+1}(x,y,z-1)}{\Delta z^2} \right) \tag{A-5}$$

Letting $\Delta x=\Delta y=\Delta z=\Delta L$, substituting Equations (A-2)-(A-5) into Equation (A-1), and collecting terms give the following linear system of equations

$$\begin{gathered} -\lambda C_i^{n+1}(x+1,y,z) - \lambda C_i^{n+1}(x-1,y,z) - \lambda C_i^{n+1}(x,y+1,z) - \lambda C_i^{n+1}(x,y-1,z) + \cdots \\ -\lambda C_i^{n+1}(x,y,z+1) - \lambda C_i^{n+1}(x,y,z-1) + (2+6\lambda) C_i^{n+1}(x,y,z) = \\ \lambda C_i^n(x+1,y,z) + \lambda C_i^n(x-1,y,z) + \lambda C_i^n(x,y+1,z) + \lambda C_i^n(x,y-1,z) + \cdots \\ \lambda C_i^n(x,y,z+1) + \lambda C_i^n(x,y,z-1) + (2-6\lambda) C_i^n(x,y,z) + r_i^n(x,y,z)\Delta t \\ \text{for} \left(1 \le x \le X\right),\ \left(1 \le y \le Y\right) \text{ and } \left(2 \le z \le Z-1\right) \end{gathered} \tag{A-6a}$$

where $\lambda=D_i\Delta t/(\Delta L)^2$. The Dirichlet boundary condition at $z=Z$ and no-flux boundary at Z=1 are accounted for by equations (A-6b) and (A-6c) respectively.

$$\begin{gathered} C_i^{n+1}(x,y,Z) = \text{Bulk Substrate Concentration} \\ \text{for all } x \text{ and } y \end{gathered} \tag{A-6b}$$

$$
\begin{aligned}
&-\lambda C_i^{n+1}(x+1,y,1)-\lambda C_i^{n+1}(x-1,y,1)-\lambda C_i^{n+1}(x,y+1,1)+\cdots \\
&-\lambda C_i^{n+1}(x,y-1,1)-2\lambda C_i^{n+1}(x,y,2)+(2+6\lambda)C_i^{n+1}(x,y,1)= \\
&\quad \lambda C_i^{n}(x+1,y,1)+\lambda C_i^{n}(x-1,y,1)+\lambda C_i^{n}(x,y+1,1)+\cdots \\
&\quad \lambda C_i^{n}(x,y-1,1)+2\lambda C_i^{n}(x,y,2)+(2-6\lambda)C_i^{n}(x,y,1)+r_i^{n}(x,y,1)\Delta t \\
&\qquad\qquad \text{for all } x \text{ and } y
\end{aligned}
\tag{A-6c}
$$

The periodic boundaries on x and y are handled by the POIS3D subroutine as discussed below. (Note: the right hand side of the equation contains only concentrations at time step *n* which are known from initial conditions or previous calculations.)

Using this method, the solution can be iterated in time to converge to the steady-state solution. The advantage to iterating the transient solution out in time is the ability to handle nonlinear reaction terms. Notice the reaction rate, r_i, is calculated at the n^{th} time step and handled naturally by a method resembling Euler's method. By assuming that the reaction rate does not change appreciably over the interval Δt (which is small), we are able to use nonlinear rate equations and apply them to only those nodes that contain biomass (i.e, r_i=0 if node is unoccupied).

Because it is the steady-state solution that is of interest in this model, we are able to use any diffusion coefficient we choose. For the simulations in Chapters 2-4 we chose the diffusivity of solute *i* in the biofilm, and choose Δt to be close to that required for stability using an explicit method (Equation 4-7).

$$
\frac{2D_i\Delta t}{\Delta L^2} \le 1 \tag{A-7}
$$

Implementation into the BacLAB Computer Model

The POIS3D subroutine solves three-dimensional block tridiagonal linear systems arising from finite difference approximations of a three-dimensional Poisson equation using the Fourier transform package (FFTPAK) written by Paul Swarztrauber. The specific system of equations solved by POIS3D is shown in Equation (A-8).

$$\begin{aligned} &H_1\left(C_i^{n+1}(x-1,y,z)-2C_i^{n+1}(x,y,z)+C_i^{n+1}(x+1,y,z)\right)+\ \cdots \\ &H_2\left(C_i^{n+1}(x,y-1,z)-2C_i^{n+1}(x,y,z)+C_i^{n+1}(x,y+1,z)\right)+\ \cdots \\ &I(z)\cdot C_i^{n+1}(x,y,z-1)+J(z)\cdot C_i^{n+1}(x,y,z)+K(z)\cdot C_i^{n+1}(x,y,z+1)=F^n(x,y,z) \\ &\qquad \text{for}\left(1\le x\le X\right),\ \left(1\le y\le Y\right)\ \text{and}\ \left(1\le z\le Z\right) \end{aligned} \tag{A-8}$$

H_1, and H_2, are constants; I, J, and K are one-dimensional constant array; and F is a three-dimensional array calculated from the initial condition or previous calculations. The constants H_1, H_2, I, J, and K are defined in the BacLAB model as

$$H_1 = H_2 = -\lambda \tag{A-9}$$

$$\begin{aligned} &I(z)=K(z)=-\lambda \quad \text{for} \quad 2\le z\le Z-1 \\ &I(1)=0 \quad \text{and} \quad K(1)=-2\lambda \\ &I(Z)=0 \quad \text{and} \quad K(Z)=0 \end{aligned} \tag{A-10}$$

$$\begin{aligned} &J(z)=2\cdot(1+\lambda) \quad \text{for} \quad 1\le z\le Z-1 \\ &J(Z)=1 \end{aligned} \tag{A-11}$$

These values equate the left-hand side of Equation (A-8) with the left-hand side of Equation (A-6). The F array is created by calculating the right-hand side of Equation (A-6) at each node point in the domain according to Equation (A-12).

$$\begin{aligned} F^n(x,y,z) = {} & \lambda C_i^n(x+1,y,z) + \lambda C_i^n(x-1,y,z) + \lambda C_i^n(x,y+1,z) + \cdots \\ & \lambda C_i^n(x,y-1,z) + \lambda C_i^n(x,y,z+1) + \lambda C_i^n(x,y,z-1) + \cdots \\ & (2-6\lambda)C_i^n(x,y,z) + r_i^n(x,y,z)\Delta t \\ & \text{for} \left(1 \le x \le X\right),\ \left(1 \le y \le Y\right) \text{ and } \left(2 \le z \le Z-1\right) \end{aligned} \tag{A-12a}$$

$$\begin{aligned} F^n(x,y,Z) = {} & \text{Bulk Substrate Concentration} \\ & \text{for all } x \text{ and } y \end{aligned} \tag{A-12b}$$

$$\begin{aligned} F^n(x,y,1) = {} & \lambda C_i^n(x+1,y,1) + \lambda C_i^n(x-1,y,1) + \lambda C_i^n(x,y+1,1) + \cdots \\ & \lambda C_i^n(x,y-1,1) + 2\lambda C_i^n(x,y,2) + (2-6\lambda)C_i^n(x,y,1) + \cdots \\ & r_i^n(x,y,1)\Delta t \\ & \text{for all } x \text{ and } y \end{aligned} \tag{A-12c}$$

The POIS3D subroutine takes 3 additional parameters to specify the boundary conditions.

$$X_{period} = \begin{cases} 0 \text{ If } C_i(0,y,z) = C_i(X,y,z) \text{ and } C_i(X+1,y,z) = C_i(1,y,z) \\ 1 \text{ If } C_i(0,y,z) = C_i(X+1,y,z) = 0 \\ 2 \text{ If } C_i(0,y,z) = 0 \text{ and } C_i(X+1,y,z) = C_i(X-1,y,z) \\ 3 \text{ If } C_i(0,y,z) = C_i(2,y,z) \text{ and } C_i(X+1,y,z) = C_i(X-1,y,z) \\ 4 \text{ If } C_i(0,y,z) = C_i(2,y,z) \text{ and } C_i(X+1,y,z) = 0 \end{cases} \tag{A-13}$$

$$Y_{period} = \begin{cases} 0 \text{ If } C_i(x,0,z) = C_i(x,Y,z) \text{ and } C_i(x,Y+1,z) = C_i(x,1,z) \\ 1 \text{ If } C_i(x,0,z) = C_i(x,Y+1,z) = 0 \\ 2 \text{ If } C_i(x,0,z) = 0 \text{ and } C_i(x,Y+1,z) = C_i(x,Y-1,z) \\ 3 \text{ If } C_i(x,0,z) = C_i(x,2,z) \text{ and } C_i(x,Y+1,z) = C_i(x,Y-1,z) \\ 4 \text{ If } C_i(x,0,z) = C_i(x,2,z) \text{ and } C_i(x,Y+1,z) = 0 \end{cases} \tag{A-14}$$

$$Z_{period} = \begin{cases} 0 \text{ If } I(1) \neq 0 \text{ and } K(Z) \neq 0 \\ 1 \text{ If } I(1) = K(Z) = 0 \end{cases} \tag{A-15}$$

The POIS3D subroutine handles the periodic boundary in x and y automatically by setting $X_{period}=Y_{period}=0$. The boundary conditions in the z direction are implemented by setting

Z_{period}=1 and assigning the proper values to I, J, and K at the boundaries as shown in Equations (A-10) and (A-11).